Atomistic Insight into the Behavior of Ions at an Oil-bearing Hydrated Calcite Surface: Implication to Ion-Engineered Waterflooding

Mohammad Hasan Badizad[1, †], Mohammad Mehdi Koleini[2, ‡], Hugh Christopher Greenwell[3],

Shahab Ayatollahi[2, *], Mohammad Hossein Ghazanfari[1]

[1] Department of Chemical and Petroleum Engineering, Sharif University of Technology, Tehran, Iran.
[2] Sharif Upstream Petroleum Research Institute (SUPRI), Department of Chemical and Petroleum Engineering, Sharif University of Technology, Tehran, Iran.
[3] Department of Earth Sciences, Durham University, Durham, DH1 3LE, UK
† **Email:** mohammadhasan.badizad@che.sharif.edu & dr.badizad@gmail.com
‡ **Email:** mmkoleini@che.sharif.edu & mmkoleini@gmail.com
*Corresponding Author; **Email:** shahab@sharif.edu & dr.ayatollahi@gmail.com

Abstract

This research provides an atomistic picture of role of ions in modulating microstructural features of an oil-contaminated calcite surface. This is of crucial importance for rational design of ion-engineered waterflooding, a promising technique for enhancing oil recovery from carbonate reservoirs. Inspired by a conventional lab-scale procedure, an integrated series of molecular dynamics (MD) simulations were carried out to resolve the relative contribution of the major ionic constituent of natural brines (i.e., Na^+, Cl^-, Mg^{2+}, Ca^{2+}, and SO_4^{2-}) when soaking an oil-bearing calcite surface in different electrolyte solutions of same salinity, namely, $CaCl_2$, $MgCl_2$, Na_2SO_4, $MgSO_4$, and pure water, DW. In all cases, we observed the gradual detachment of polar oil molecules (mimicked by decanoate) already paired to Na^+ cations covering the calcite substrate, in a way that carboxylate groups gathering in contact with the treating solution. The appearance of such a negatively charged interface in conjunction with the bare calcite/brine surface is a likely nanometric source for the disparity of surface characteristics of oil-bearing rocks reported in the literature. MD results showed the affinity of divalent cations (Ca^{2+} or Mg^{2+}) for pairing with negatively charged carboxylate functional groups and thereby, facilitating desorption of decanoates. Having a compact solvation shell, Mg^{2+} was not as effective as Ca^{2+} cations, however, its performance was enhanced in the presence of sulfate anions. We further figured out the tendency of SO_4^{2-} anions to shielding Na^+ sites over the calcite surface, thus limiting the chance of re-adsorption of carboxylate compounds. Consistent with lab experiences, sulfate was found to assist the access of magnesium cations to the calcite surface as well. Altogether, the present results provide us with a molecular-level validation for the well-known multi-component ions exchange mechanism proposed for the wettability alteration of carbonate rocks through enriching the divalent ionic content of the injection brine solution.

Keywords: Ion-engineered waterflooding; Molecular dynamics simulation; Calcite; Interface; Adsorbed organic material; Aqueous solution; Ion pairing.

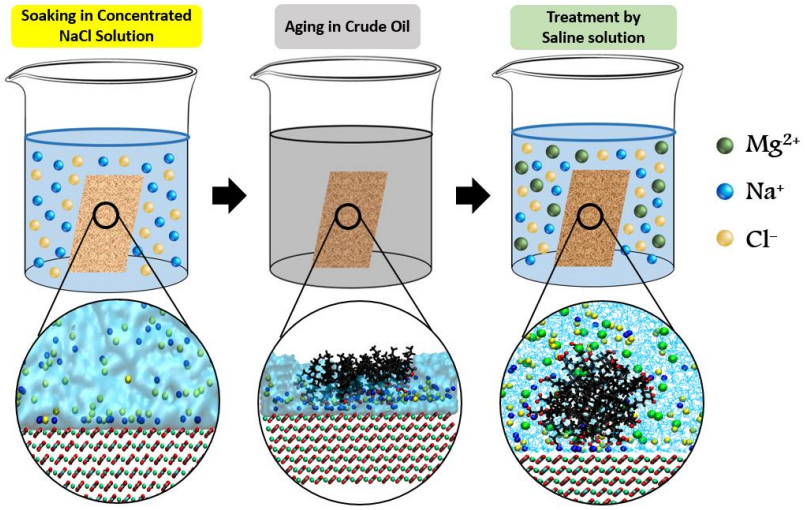
Soaking in Concentrated NaCl Solution
Aging in Crude Oil
Treatment by Saline solution
Mg^{2+}
Na^{+}
Cl^{-}

Introduction

Mineral/hydrocarbon/brine interface systems are ubiquitous in diverse natural environments and industrial applications, *e.g.*, migration and deposition of organic contaminants in underground aquifers, enhanced oil recovery, *inter alia* [1]. Competitive affinity of different species (ions and dissolved organic compounds) for accumulating at an interface is of importance to many areas of surface science [2,3]. For instance, lab experiences have unanimously confirmed the ion-sensitivity wettability response of carbonate rocks while treating at a same salinity level [4]. In this regard, ion-engineered waterflooding has been applied as an effective technique for improving oil recovery from carbonate reservoirs [5–9]. In this operation, an electrolyte solution with modified ionic composition is injected into a candidate petroleum reservoir in order to enhance oil recovery through shifting naturally oil-loving rocks to a more water-wet state [10]. Wettability modification of carbonate reservoirs in that process is known to be driven by the so-called potential determining ions (Ca^{2+}, Mg^{2+}, and SO_4^{2-}), which tend to facilitate release of surface active compounds of crude oil, mostly composed of carboxylic acids, from the pore walls [11].

Despite the strongly hydrophilic virtue of carbonate crystals [12], a wide spectrum of wettability has been reported for carbonate sediments in petroleum basins and marine environments [13]. It has been argued that adsorbed organic materials render the pore surface of carbonate rocks to an oil-favoring state [14]. Polar molecules, particularly carboxylic ones, adhere so tightly that X-ray diffraction (XRD) spectroscopy and atomic force microscopy (AFM) have confirmed the existence of hydrocarbons spots persisting on the pore walls even after solvent-flushing of oil-bearing rock samples[15]. The presence of organic impurities has also been identified through the differing force maps of treated and fresh rock surfaces obtained by chemical force microscopy (CFM) measurements [16].

Molecular dynamics (MD) simulation has been widely employed in various fields of science and technology in order to unravel the physicochemical aspects of interfaces at nanometer

resolution [17,18]. In this respect, Underwood et al. applied MD simulation to ascertain importance of ion exchange mechanism in adsorption process of charged and neutral acidic compounds on clay minerals [19]. They further explored the clay-organic interaction by focusing on the affinity of decane, decanoic acid and decanamine to hydrated kaolinite. It was concluded that ionic interactions dominate surface adsorption of those surface-active compounds [20]. Regarding calcite/brine systems, Zhao et al. investigated the mobility of apolar hydrocarbons enclosed within a calcite nano-slit. The study found the determining impact of NaCl salinity on the wetting state of the nano-pore to be insignificant [21]. In later work, the salinity-dependent deformation of a nanodroplet of n-decane on a calcite substrate was studied, and a reduction of contact angle correlated with increasing salt concentration of the aqueous environment [22]. Recently, Koleini et al. observed a direct relationship between extent of benzoic acid adsorption onto calcite and concentration of sodium cations in the aqueous interface region [23]. They also pointed out importance of ion-pairing in the brine film separating hydrocarbon phases and pore wall of carbonates [24]. Molecular simulation revealed the ability of ionic clusters in stabilizing brine film [25].

As reviewed above, molecular simulation has paved the way for fundamental research on interactions involved in ion-engineered waterflooding. However, we are at the beginning stage and there is a far route to fully scrutinize all nanoscopic phenomena. To the author's knowledge, there has, hitherto, been no report in the open literature concerning the time-evolution of the microscopic characteristics of a hydrocarbon-bearing calcite substrate exposed to a saline solution. Prior relevant MD investigations have been devoted to equilibrium state studies of oil-rock-brine systems. Moreover, the individual and concomitant behavior of divalent ions in the calcite/hydrocarbon/brine interface are not fully understood at a molecular level yet. Motivated by this lack of knowledge, the current research seeks to shed light on the contribution of ions to calcite-brine interface in presence of adsorbed organic matter (AOM). For this purpose, an integrated atomistic investigation was carried out here to

probe, at atomic-level resolution, the structural evolution of a hydrated calcite substrate with polar AOM, soaked in various electrolytes solutions. We specifically address the spatial distribution and localization of ions over time, interacting with the bare mineral surface and AOM. Throughout, the ion-specific adsorption affinity of polar hydrocarbons on calcite surface was especially scrutinized. It was attempt to provide microscopic interpretation for empirical observations and evidence in the literature. The remainder of this paper is organized as follows: (i) in the next section we will concisely explain the model construction and simulation methodology; (ii) this is followed by a analyzing the evolution of the calcite/oil/brine system in terms of preferential interaction and distribution of different species; (iii) then, we discuss and compare effect of different soaking electrolyte solutions, highlighting the connection between MD results and what commonly observed in macro- and nanoscopic experimental investigations as well as previous computational works; (iv) the paper will be concluded by summarizing key findings.

Simulation methodology

Model Setup

The simulation protocol taken here was inspired by an experimental procedure conventionally carried out in laboratory investigations for examining surface characteristics of solid substrates in an aqueous environment of known chemistry [26–28]. A polished (finely smooth) thin slice of known mineralogy is initially soaked in a concentrated brine solution (with typical salinity of 100,000-300,000 ppm [29]) to establish the equilibrated original state of rock/brine interfaces in subsurface aquifers. The solid sample is then, generally, dried carefully such that preserving the moisture due to surface hydration. By doing so, it is expected to have a thin wetting layer of saline solution remained on the solid surface. At the next stage, aimed at mimicking the exposure of the rock surface to organic components, a process that naturally happens upon oil migration into subsurface reservoirs or leakage of hydrocarbon-based

contaminants into aquifers, [30] the sample is aged in a sealed crude oil container to allow penetration of organic molecules through the brine film, hence adsorbed onto the solid surface. This process often shifts the wetting state of the crystalline samples from strongly water favoring to neutral- (or even oil-) wet condition [13]. Thereby, we come up with a solid surface covered by a uniform thin brine film together with sporadic hydrocarbon patches, which has been evidenced by nanoscale high resolution AFM observations [14,15,31–34]. Finally, the oil-aged slab is immersed in an aqueous solution. Various techniques are then applied to analyze the impact of fluid chemistry on the characteristic features of the mineral surface.

Following the procedure described above, a systematic simulation strategy was here devised to resolve in atomic detail the microscopic features of an oil-bearing calcite surface treated by different electrolyte solutions. An orthorhombic calcite substrate of dimensions 5.7×5.5×1.9 nm^3 was built by cleaving and replicating a unit cell of $CaCO_3$ along the plane $(10\bar{1}4)$, with crystallographic coordinates taken from American Mineralogist Crystal Structure Database [35]. The unit cell dimensions are long enough to avoid possibly self-interaction of atoms through period boundaries because of the minimum-image convention applied in our computational study [36].

As shown in **Figure 1.1** , the space above the calcite surface was filled with a 6 nm-thick NaCl solution of 3.0 $mol.dm^{-3}$ salinity (*i.e.*, ~175,000 ppm) and the resulting system was then equilibrated at 300.0 K (corresponding to the normal laboratory conditions) for 20.0 ns. It was learned from our previous publications that sodium cations are necessary for adsorption of negatively-charged oil compounds, typically carboxylates, on a hydrated calcite surface [37], *i.e.,* no surface adsorption will happen for an ultra-pure water in contact with a calcite slab. Also note that we expect a stable calcite/water interface during conventional MD experience because of limited accessible time (a few nano seconds) and very low solubility of $CaCO_3$ mineral [37]. AFM survey by Ricci et al. also supports the uniformity of a nano-sized calcite surface in contact with an aqueous solution [38].

Afterwards, the water molecules and accompanying ions were excluded from the fluid phase to leave a 1 nm-thick brine film over the calcite substrate (**Figure 1.2**). Care was taken to maintain charge balance of the system. The thin brine film was comprised of only NaCl, due to the abundance of that electrolyte in groundwater aquifers and marine solutions [39].

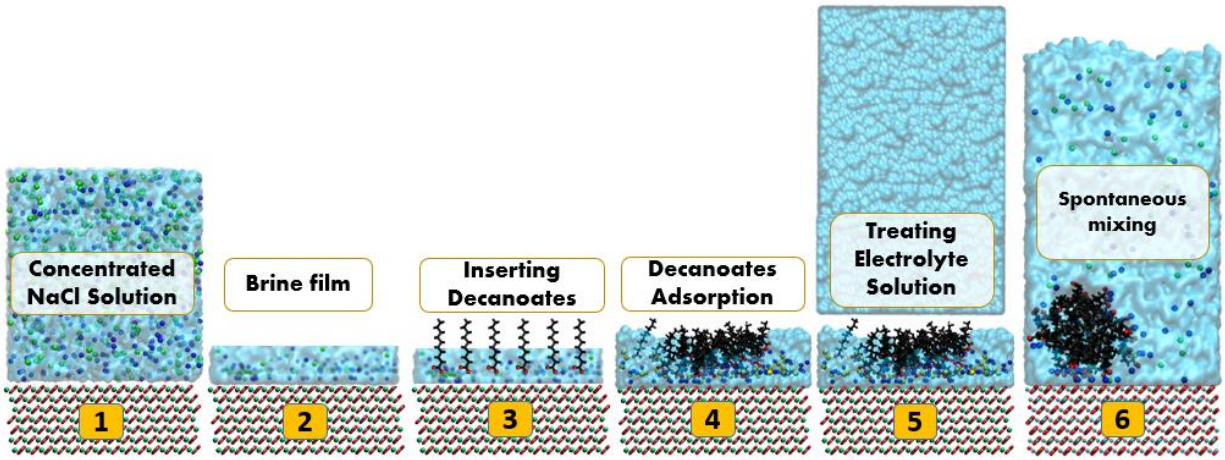

Figure 1 Schematic description of the simulation protocol: (1) equilibrating a $CaCO_3$ slab in contact with a 6 nm thick concentrated (3.0 mol.dm^{-3}) NaCl solution; (2) removing water molecules and associated ions leaving a thin brine film over the solid substrate; (3) inserting decanoate molecules into the brine film; (4) an oil clump develops by surface adsorption and self-aggregation of decanoate; (5) placing a 9 nm thick single electrolyte solution (NaCl, $CaCl_2$, $MgCl_2$, Na_2SO_4, or DW) immediately over the water film; and finally (that is the main stage) (6) allowing diffusive transport of ions within the aqueous environment along with the conformational variation of the residing decanoates.

In the next step, decanoate molecules ($C_{28}H_{44}O_3$) representing polar oil components were partially inserted into the brine film to uniformly cover the calcite surface, while standing parallel to each other (**Figure 1.3**). Prior to progressing the simulation, water molecules overlapping (or very close) to decanoate molecules were eliminated to avoid instability due to excessive repulsion in the system. Excess sodium cations were introduced to the brine solution in order to satisfy the charge neutrality of the system. The simulation was run for 20.0 ns to allow adsorption and assemblage of decanoate molecules (**Figure 1.4**). Adequacy of the simulation timespan is discussed in section S1 of the Supporting Information. Note that decanoic and other aliphatic acids have been widely utilized both in experimental and theoretical studies to represent the polar fraction of crude oil [40]. It has been well recognized

that surface activity of organic molecules (*i.e.*, tendency for accumulation at aqueous interfaces) is mainly driven by carboxylic acid (-COOH) and hydroxyl (-OH) functional groups [41]

Since pH cannot be directly imposed *a priori* in classical MD simulations, we should necessarily consider an atomic model in close correspondences to actual lab conditions. Since a $CaCO_3$/water system buffers to pH = 8 at ambient laboratory-scale measurements [42], decanoic acid (with pKa = 4.9) is expected to fully deprotonate into decanoate (*i.e.*, -COOH becomes $-COO^-$) [43] in an aqueous media. As such, decanoate is a reasonable candidate for representing hydrocarbon compounds adhered on a hydrated mineral surface. Regarding the calcite substrate, the prevailing pH conditions of normal lab practices coincide with iso-electric point of $CaCO_3$, revealed by zeta potentials measurements [44]. Therefore, the inherent charge neutrality of $CaCO_3$/water interface taken here is in accord with typical experimental conditions. We should also note that the origin of pH-sensitivity of carbonate surfaces is not yet clearly resolved [44]. This explains the inability of the commonly used $CaCO_3$ force-fields for incorporating the impact of pH variation.

To model the soaking process, a pre-equilibrated 1.0 $mol.dm^{-3}$ single electrolyte solution (either $CaCl_2$, $MgCl_2$, Na_2SO_4, $MgSO_4$, or deionized water, DW) with a thickness of 9.0 nm was placed just over the oil-brine layer that covers the calcite surface (**Figure 1.5**). $CaSO_4$ was ignored because of having a very low saturation concentration, much below the salinity level considered here (1 $mol.dm^{-3}$) [3].

In the next section, we evidence that the contacted solutions are thick enough to account both for interface and bulk space. In all cases, a large vacant space of height ~10.0 nm was placed above the soaking brine to avoiding unwanted interaction of the solution and calcite slab through the periodic boundary along the z-direction. Throughout, we effectively model the solution/vapor equilibrium by applying NVT ensemble, a practice which has been commonly followed in former investigations [6,45].

The chosen electrolytes include the major electrolyte content of natural saline solutions, that is Na^+, Cl^-, Ca^{2+}, Mg^{2+}, and SO_4^{2-}, which have been described as wettability-determining ions because of their noted abilities in altering surface charge and adsorption tendency on siliceous and carbonate rocks [46]. The simulation was performed at 300.0 K for each treating solution and the motion of fluid components was traced for 100.0 ns (**Figure 1.6**). All of the configurations were created using the PACKMOL program [47] , where the number of water molecules was initially set to achieve the density ~1.0 g.cm^{-3}.

Computation details

All atomistic computations were performed using the LAMMPS package. This open source software provides the possibility to trace the evolution of a particle-based system by integrating classical Newton's equations of motion for constituting particles based on the velocity-Verlet scheme [48]. Integration was carried out numerically at discrete time steps of 1.0 fs. The $CaCO_3$ substrate was modeled by the force field developed by Xiao et al. [49], which has attained accuracy and validity for studying surface adsorption of ions and hydrocarbons onto calcite surfaces [50–52]. Decanote molecules were represented by the OPLS-AA parameterization, wherein the van der Waals potential is account for by a Lennard-Jones 12-6 expression within the cut-off radius of 1.0 nm [53]:

$$E_{LJ} = \left[\frac{A}{r_{ij}^{12}} - \frac{B}{r_{ij}^{6}}\right], \quad (1)$$

where two atoms *i* and *j* are at a distance r_{ij} apart. The LJ parameters (*A* and *B* in eq. 1) of unlike atoms, *i* and *j*, were deduced using the geometric combination rule, that is, $A_{ij} = \sqrt{A_{ii}A_{jj}}$ and $B_{ij} = \sqrt{B_{ii}B_{jj}}$ [53]. Short-range component of electrostatic interactions were calculated in real-space and long-range forces were resolved in the reciprocal space by applying the particle-particle/particle-mesh (PPPM) method, with a precision of 10^{-5}.

The intra-molecular potentials, namely, bond stretching, angle bending, and dihedral torsion were represented respectively as follows [53]:

$$E_{bond} = \sum_i K_i^r (r_i - r_{i0})^2 \quad (2)$$

$$E_{angle} = \sum_i K_i^\theta (\theta_i - \theta_{i0})^2 \quad (3)$$

$$E_{dihedral} = \frac{1}{2}\sum_i \sum_{n=1}^{4} K_{n,i}^\varphi [1 + (-1)^{n+1} cos(n\varphi_i)] \quad (4)$$

where r_0, θ_0, φ_i stand for equilibrium bond lengths, angles, and dihedral angles, with stiffness coefficients of K^r, K^θ and K_n^φ, respectively. Force field parameters used in this work are listed in section S2 of the Supporting Information.

All simulations were conducted under NVT (constant number of particles (N), constant volume (V), and constant temperature (T)) ensemble by coupling the system to a Nose-Hoover thermostat with a damping constant of τ = 0.1 ps. By applying NVT ensemble in this setup, it is assumed that the aqueous phase is in equilibrium with vapor at the specified temperature, 300 K. Due to having solid (crystalline) phase, it is not viable to set pressure by coupling the whole system to a barostat under NPT ensemble.

Periodic boundary conditions were imposed in the x, y, and z directions. The simulation box dimensions were set to 5.7×5.5×36.0 nm^3, such that two large vacuum spaces exist at the top and bottom of the physical model to avoid unwanted interaction through period images and also preventing water molecules from flying out. Atomic trajectories were collected every 1.0 ps for post-simulation analysis.

Results

In this section, the microscopic characteristics of the calcite/hydrocarbon/brine system were evaluated for each contacted electrolyte solution. Various analyses were carried out to quantify and compare the distribution and pairwise interaction of ions and hydrocarbon over time. Before proceeding further, the mean square displacement (MSD) of ions was calculated over the course of each simulation to ensure the adequacy of timeframes, using the following expression [53]

$$MSD_{\alpha}(t) = \frac{1}{N}\left\langle \sum_{i=1}^{N} \left| r_{\alpha,i}(t + t_0) - r_{\alpha,i}(t_0) \right|^2 \right\rangle_{t_0} \quad (5)$$

with $r_{\alpha,i}$ denoting the spatial position of a particle *i* along the α-direction. Angular brackets mean the ensemble average of the enclosing expression over different reference timesteps, t_0. The summation runs over total number of particles, *N*. **Figure S5** exhibits the linearly time-varying MSD diagrams of ions parallel to the calcite surface (*i.e.*, MSD_x and MSD_y), demonstrating the lateral diffusive propagation of ions. Conversely, the vertical component of the MSD diagram (MSD_z) flattens out at approximately 20 ns following a linearly varying sub-diffusive regime. This naturally arises due to the restricted movement of ions perpendicular to the calcite slab, *i.e.* along the z-axis. Generally, all systems were judged to achieve equilibrium at about 60.0 ns.

Deionized Water (DW)

The time-evolution of solid-brine interface exposed to DW are reported in **Figure 2**. It can be seen that ions (Na^+ and Cl^-) steadily leave the calcite interface and dissolve into the overlying pure water phase. During the dilution process, the decanoate clump reshapes by successive detachment of carboxylate functional groups from the calcite surface, turning into a micelle-like entity consisting of a hydrophobic core of aliphatic chains with negatively-charged carboxylates facing outwards to the aqueous phase. It is apparent from the given snapshots (**Figure 2**) that, sodium cations, accumulated adjacent to the calcite slab, would serve as adsorption sites for carboxylate groups, which was also pointed out in our previous publication [23]. Besides visual inspection, the conformational evolution of the oil clump was quantitatively represented by radius of gyration, R_g [54]. The formulation details and computational results are presented in **section S3** of the **Supporting Information**. For all soaking solutions shown in **Figure S6**, R_g begins to vary from a same initial value, ~ 8.0 Å, and then reaches a stabilized value indicating structural equilibration of the decanoate aggregate. For the case of DW solution, **Figure S6** displays a relatively noisily variation of R_g within early 30 ns of the process

and then oscillating around ~ 7.0 Å. The time-varying profile of R_g for other treating solutions will be discussed later in the corresponding subsections.

Two near-surface peaks were distinguished in the concentration profile of sodium (**Figure 3**) at 2.9 and 5.5 Å, due to direct and solvent-separated binding of Na^+ cations to the solid surface, respectively. As shown in the corresponding snapshots (insets), sodium cations in aqueous solution couple with the protruding oxygen atoms of basal carbonates on the calcite surface. In line with the surface loading of sodium cations, two peaks were recognized in the carboxylate distribution plot at 5.0 and 7.7 Å (**Figure 4**). This implies that carboxylate adsorption was governed by pairing of $–COO^-$ groups with Na^+ cations already located on the calcite surface, as elucidated by the inset in **Figure 4**. By ion pair, we means association of two negatively charged ions as a result of electrostatic attractive force between them. Note that carboxylate groups were spatially described by the carbon bonded to oxygen atoms. Based on the carboxylate distribution plot, the hydrocarbon-occupied space can be conceptually partitioned into two interface regions normal to the solid surface, as schematically illustrated in the inset of **Figure 4**. This partitioning allows us to distinguish the behavior of ions and carboxylate in the vicinity of the calcite surface and at the upper portion of the oil mass. Distribution diagram of the tail of decanoate molecules, i.e., methyl group ($-CH_3$), is plotted for different treating solution in **Figure S7** of the **Supporting Information**. This complementary analysis provides an indirect confirmation for having approximately two distinct interfaces: one due to attachment of decanoates on the calcite surface and the other developed by desorbed decanotes contacting the soaking solution. This bifurcations is mirrored to a clear peak, mid-way in the density plot of methyl groups, ~ 15.5 Å. The same holds for all treating solutions, shown in **Figure S7**.

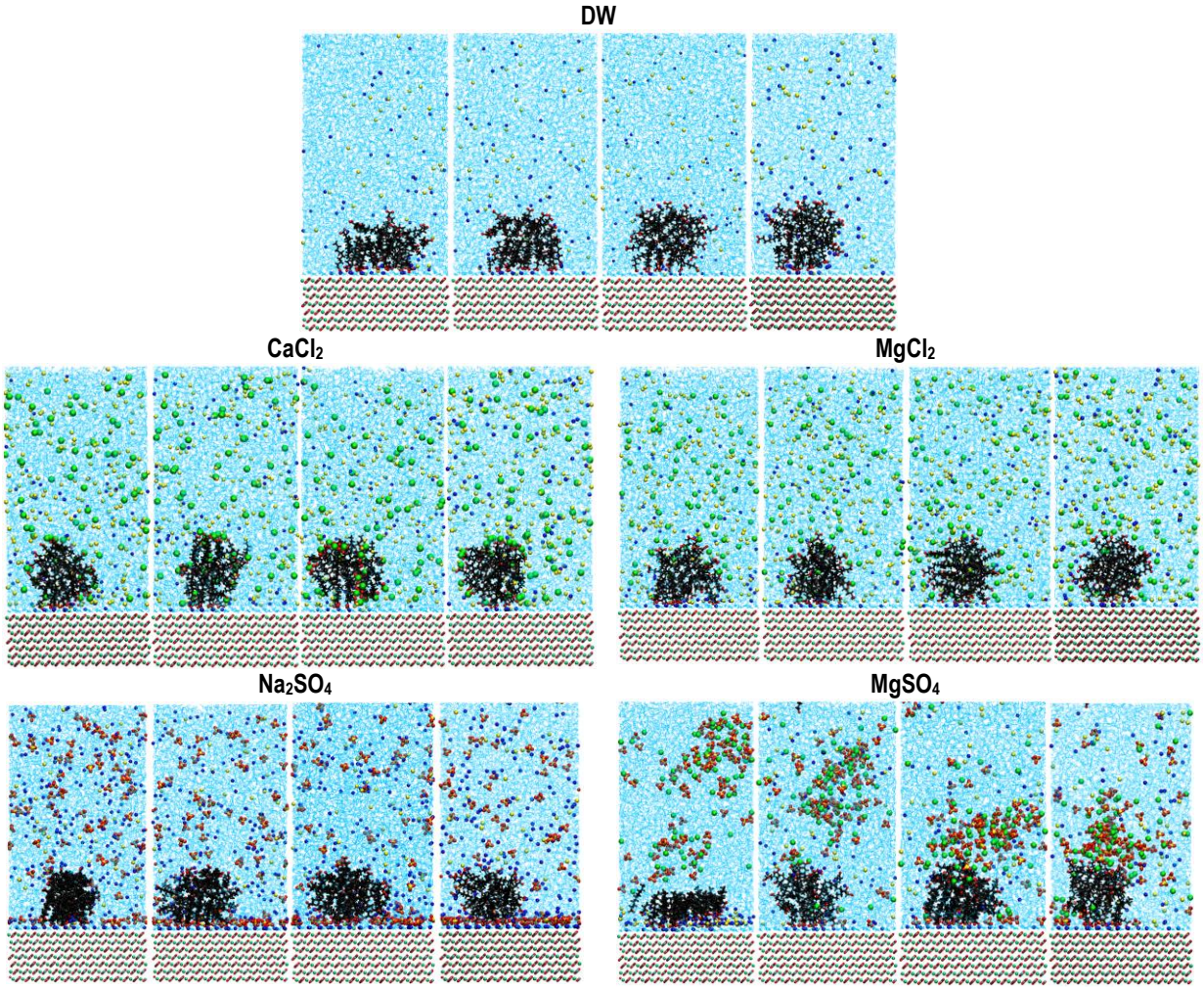

Figure 2 Representative snapshots, taken at labeled instances, of the hydrocarbon-bearing calcite slab exposed to various electrolyte solutions. Color codes: sodium, blue; calcium and magnesium, green; chloride, yellow; aliphatic chain, black; oxygen, red; sulfur, creamy; calcium in calcite, green; water, scattered blue.

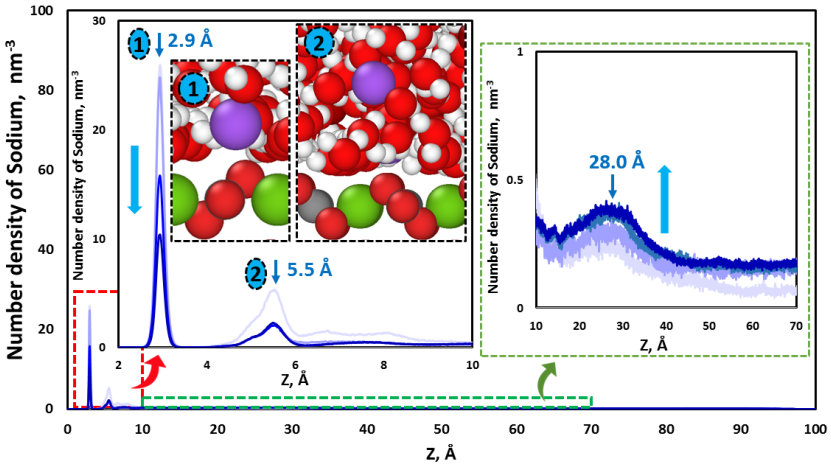

Figure 3 Distribution diagram of sodium cations along the z-direction, *i.e.*, perpendicular to the calcite basal plane, when treated by DW. Light to dark blue diagrams belong to statistics gathered at successive timespans: 0-10 ns, 10-30 ns, 30-60 ns, and 60-100 ns. The delimited domains are closed up in corresponding insets. Two peaks distinguished in the left inset belong to different modes of sodium adsorption illustrated by given snapshots: (1) contact ion-pairing of Na^+-carbonate at 2.9 Å; and (2) solvent-separated Na^+-carbonate pairing at 5.5 Å. Right inset highlights accumulation of Na^+ ions over the oil patch centered at 28.0 Å. The blue arrows display the general (ascending or descending) trend of the profiles in each zone. The color codes are mentioned in **Figure 2**.

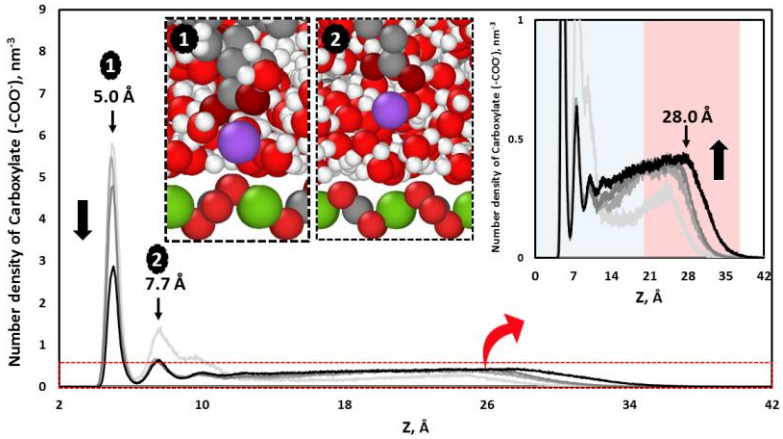

Figure 4 Distribution profile of the carboxylate groups along the z-axis (normal to the calcite plane) upon using DW. Light to dark black diagrams belong to statistics collected at successive timespans: 0-10 ns, 10-30 ns, 30-60 ns, and 60-100 ns. Note that carboxylate was spatially described by the position of the carbon bonded to oxygen atoms. Insets exhibit the representative snapshots for the corresponding specified domains. Two peaks distinguished in the calcite neighborhood belong to binding of carboxylate to different types of residing Na^+ cations, illustrated by given snapshots. Right inset highlights accumulation of carboxylate groups and sodium cations at top of the oil patch centered at 28.0 Å. It also demonstrates conceptual partitioning of the hydrocarbon-occupied zone into upper and lower interface regions. The black arrows display the general (ascending or descending) trend of the profiles in each zone. The color codes are mentioned in **Figure 2**.

The RDF profiles given in **Figure 5** further confirms favoring carboxylate-sodium pairing near the calcite slab surface. Note that a special procedure [8,55,56] was adopted for calculating RDF profiles because of our atomic system not being spherically symmetric. To do so, RDF plots were obtained by counting and averaging pairs of particles within a semi-spherical cone space on the calcite surface. In this graph, the shoulder-shaped peak denotes the monodentate and bidentate modes of carboxylate-sodium association (note insets in **Figure 5**), while the second peak belongs to the water-mediated contact. Overall, one can think of this adsorption mechanism as if a Na^+ cation was shared between a carboxylate group and a protruding oxygen of carbonate. There is a close relationship between the distribution diagrams of sodium and carboxylate (**Figures 3-4**): in both cases, the near-surface adsorption layers descend steadily and simultaneously over time. This is mirrored in the time-decreasing COO^--Na^+ RDF profile (**Figure 5**) as well. **Figure S8** shows the decreasing fraction of sodium cations detected within the near interface region by the end of ~25.0 ns to stabilize at a surface concentration (*i.e.,* coverage) of 4.0 nm^{-2} (**Figure 6**). For the sake of completeness, the fraction of ions entered to the upper interface region is plotted for all treating solutions in **Figure S9**. It is seen that Na^+ cations and carboxylate groups, steadily and simultaneously, appear at the oil/water interface at the top of oil clump.

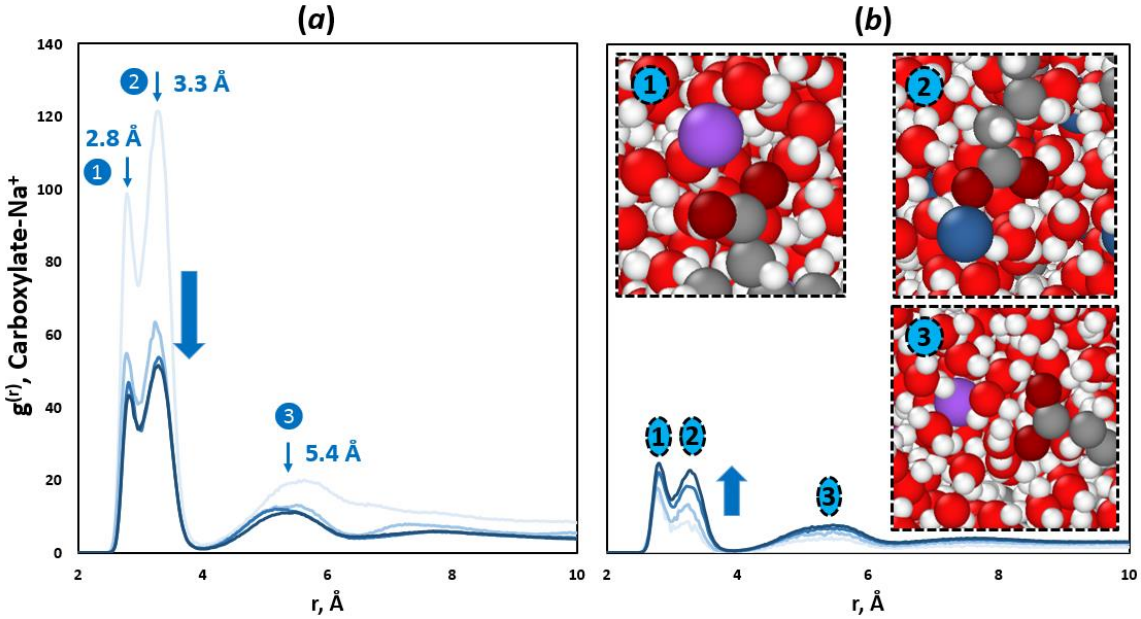

Figure 5 Radial distribution function, $g^{(r)}$, of carboxylate-Na^+ interaction within the bottom (panel *a*), and top (panel *b*) interface regions in case of using DW. Diagrams were obtained using statistics gathered at successive timespans, namely, 0-10 ns, 10-30 ns, 30-60 ns, and 60-100 ns, shown by light to thick blue profiles, respectively. The peaks labeled in panel (*a)* are due to: (1) bidentate; (2) monodentate; and (3) solvent-separated pairing of carboxylate-Na^+, as illustrated in the panel *b*. Blue arrows indicate the general (descending or ascending) time-evolution trend of the RDF profiles. The color codes are as given in **Figure 2**.

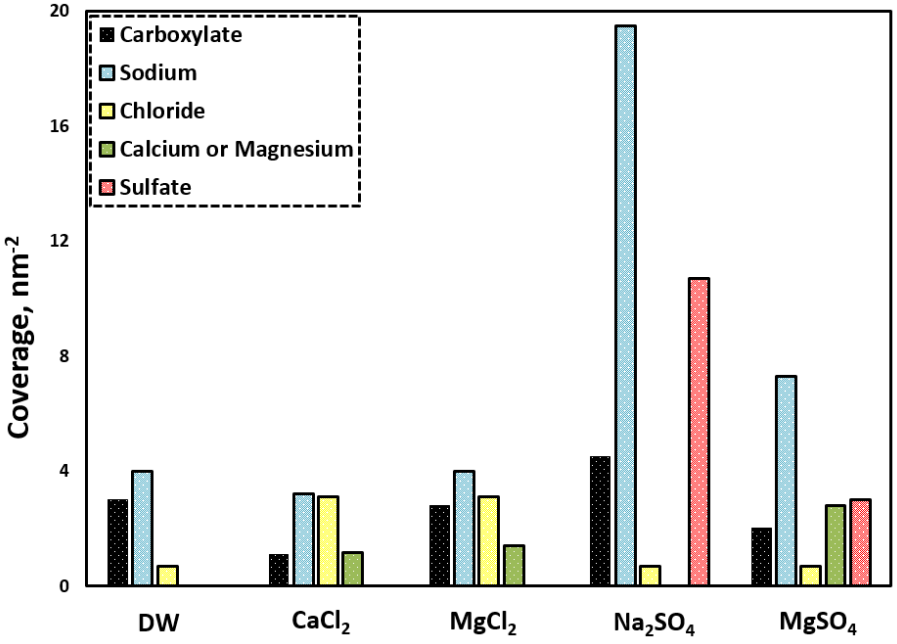

Figure 6 Surface coverage density of ions and carboxylate on the calcite substrate at equilibrium state for various salts tested.

Figure 4 shows that the AOM extends from the solid slab to approximately Z=35.0 Å. A broad peak is noticed in the density diagram of carboxylate centered at 28.0 Å, which stems from the crowding of carboxylates in contact with the soaking aqueous solution. This reveals that a rugged negatively-charged oil-water interface arose at the top portion of the AOM. This emergent interface attracted Na^+ cations released from the solid surface, already noticed from the evolving peak at ~ 28.0 Å in the distribution profile of sodium ion (**Figure 3**). The rising RDF profiles (**Figure 5.b**) show the progressive interaction of Na^+ cations with carboxylates at top of the decanoate aggregate.

Analogous to Na^+ ions, chloride anions tend to concentrate nearby the calcite surface. It was pointed out in our previous investigations that a compact layer of Na^+ cations attracts Cl^- ions towards the calcite slab [9,57]. As such, chloride-sodium pairs will develop next to the calcite surface. Surface accumulation of Cl^- anion is readily recognized through three peaks in the density distribution profile of that ion at 2.8, 5.0, and 7.4 Å (**Figure S10**). On the basis of the sodium distribution plot (**Figure 3**), the primary and secondary peaks in chloride distribution diagram (**Figure S10**) are due to the sitting of a chloride ion alongside and above an already lodging Na^+ cation, respectively, and the third caused by solvent-separated ion pairing (SSIP). Given Na^+-bridge surface binding of chloride ions, we observe the substantial desorption of those anions from the surface upon migration of sodium cations away from the calcite-water interface. It is seen in **Figure 6** that surface concentration of Cl^- ions reduced to ~0.7 nm^{-2} in parallel to that of Na^+ cations, both reaching a plateau within the early ~25.0 ns (**Figure S10**). However, in comparison to Na^+ cation (**Figure 2**), there is a scarcity of chloride anions within the AOM-occupied region, most likely because of the electrostatic repulsion induced by carboxylate groups around the AOM.

$CaCl_2$ solution

As in the case of DW discussed above, using $CaCl_2$ brine disturbs the aggregated decanoate molecules residing on the calcite slab, as revealed graphically in **Figure 1**. The near-surface

environment becomes diluted through transport of the indigenous sodium and chloride ions into the bulk electrolyte solution. In particular, calcium cations concentrated around the decanoate droplet. This contrasted with the treatment by DW, in which the decanoate aggregate was screened by Na^+ cations liberated from the mineral-water interface (**Figure 2**). Regarding gyration of radius, reported in **Figure S6**, we notice the gradual and monotonic increasing trend of R_g for the decanoate aggregate in contact with the $CaCl_2$ throughout the treating process. This evidence quantitatively highlights the slight inflation of the oil clump in response to being uniformly surrounded by Ca^{2+} cations.

From the statistics gathered over successive timeframes (**Figure 7.a**), the decanoate aggregate underwent an immediate restructuring by surface detachment of some decanoates during the initial 30.0 ns. Release of carboxylates from the surface was accompanied by closer accumulation of those functional groups in contact with the $CaCl_2$ solution, as evidenced by the subtle peak in the early 10.0 ns of the carboxylate distribution plot, centered at approximately 28 Å (**Figure 7.a**). Throughout, $-COO^-$ head groups gradually distributed to uniformly appear within the region occupied by the AOM. This analysis, in conjunction with the snapshots given in **Figure 1**, leads to the conclusion that carboxylates tended towards evenly distributing spatially around the hydrocarbon patch periphery, under the $CaCl_2$ brine. Extra desorption of decanoates from the calcite surface was noted when introducing the $CaCl_2$ brine, compared to using DW, with coverage values of 1.1 against 3.0 nm^{-2}, respectively (**Figure 6**).

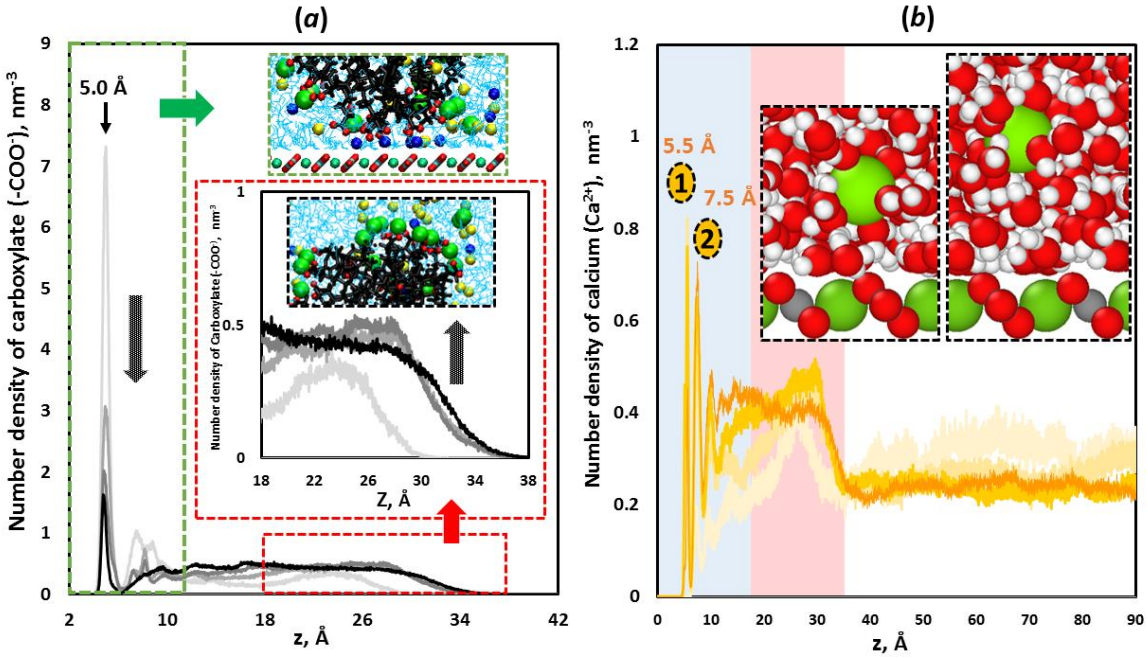

Figure 7 Number density distribution of (*a*) carboxylate, and (*b*) calcium cations along the z-direction when using $CaCl_2$. Light to dark profiles belong to statistics collected at successive timespans: 0-10 ns, 10-30 ns, 30-60 ns, and 60-100 ns. Insets in panel (*a*) are of the domains delimited within the dashed rectangles. The magnified image of the specified domain as well as pertaining snapshots are included as insets in panel (a). Insets in panel (*b*) schematically illustrate localization and hydration of Ca^{2+} cations in the distinguished adsorption layers. Regions highlighted in blue and red in panel (*b)* indicate lower and upper interfaces, respectively, as defined in **Figure 4**. Black arrows show the general (descending or ascending) time-evolution trend of the carboxylate profiles.

Ca^{2+} cations primarily concentrated over the oil patch during the early stages of the simulation process (*i.e.*, 0.0-30.0 ns) and, afterwards, steadily approached the calcite slab surface, evenly dispersing around the AOM (**Figure 7.b**: notice the region highlighted in red). Evidently, Ca^{2+} cations distributed in the system closely paralleling the spatial evolution of carboxylates (**Figure 7.a**). Two sharp peaks were distinguished in the concentration diagram of Ca^{2+} (**Figure 7.b**), reflecting the preferential binding of that cation to the calcite surface at 5.5 and 7.5 Å, respectively. Compared to the direct adsorption of Na^{+} at 2.9 Å (**Figure S11**), our results demonstrate that Ca^{2+} arranged at a greater distance from the calcite surface. As shown in the insets in **Figure 7.b**, calcium cations resided over the calcite surface by forming outer-sphere complexes. Surface adsorption of Ca^{2+} cations is mediated by water molecules. Generally, calcium ions tended to accumulate within the region occupied by the decanoate

aggregate (z = 4.0 to 35.0 Å), with a concentration larger than the bulk solution (*i.e.*, where Z > 40.0 Å). Conversely, **Figure S11** illustrates the greater concentration of Na^+ ions within the bulk space. It was observed that Na^+ concentration varies within z= 20.0-37.0 Å from low (0.16 nm^{-3} in the AOM region) to high (0.23 nm^{-3} in the bulk space) values. Conceptually, one might think of an ion exchange process whereby the in situ Na^+ leaves the calcite surface, with Ca^{2+} simultaneously being drawn into the AOM-occupied region until achieving equilibration by the end of ~30.0 ns (**Figure 9**).

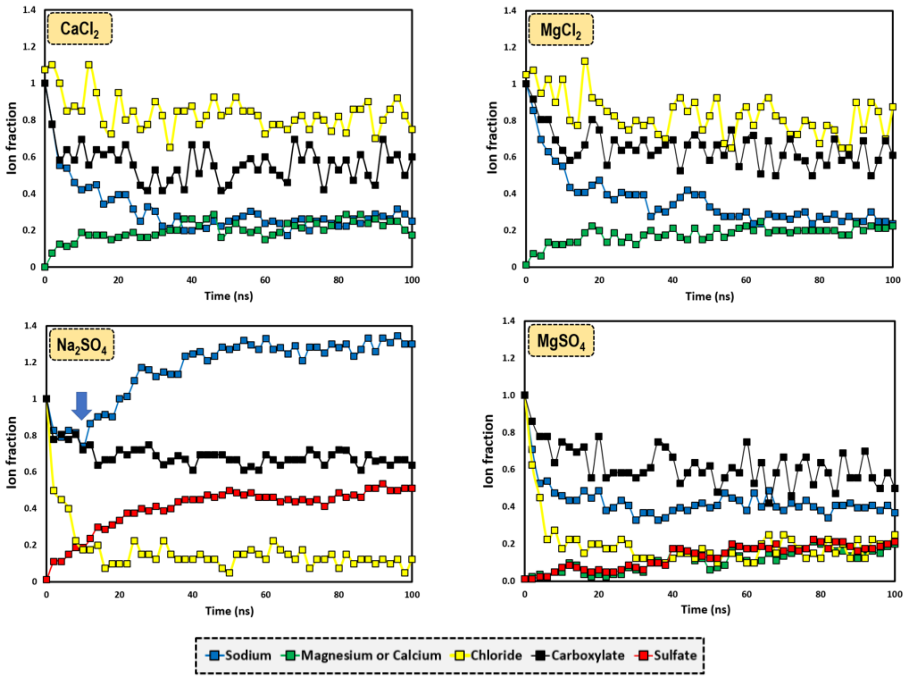

Figure 8 Time-varying fraction of ions and carboxylates detected within the bottom interface region for different saline solutions (note labels).

The distinct behavior of Ca^{2+} and Na^+ cations possibly arises from their different affinities to carboxylate groups. The sequence of snapshots presented in **Figure 2** suggested that $–COO^-$ favored association with the incoming diffusing Ca^{2+} cations over the *in situ* Na^+ ions, resulting in decanoate molecules paired with divalent cations. This visual deduction is quantitatively verified by comparing carboxylate-Ca^{2+} and $–Na^+$ RDF plots (**Figure 9**). The higher peaks of the carboxylate-Ca^{2+} RDF plots reflect the preferential association of calcium cations with

carboxylate head-groups, both at the bottom and top of the AOM. Moreover, RDF profiles obtained at consecutive timeframes (**Figure 9**) demonstrated the increasing and decreasing extent of carboxylate interaction with Ca^{2+} and Na^{+} cations, respectively. From a physical perspective, Ca^{2+} cations coming from the soaking solution develop ion pairs with carboxylates, replacing the pre-associated Na^{+} cations, especially those anchoring decanoate molecules to the calcite surface. This process, facilitating the decanoate desorption from the surface, explains the greater desorption of decanoates upon using the $CaCl_2$ solution compared to DW, with a final surface concentration of 1.5 *vs.* 3.0 nm^{-2}, respectively (**Figure 6**). The additional detachment of carboxylates when using $CaCl_2$ solution is accompanied by the release of additional Na^{+} cations from the surface compared to the case of DW (**Figure 6**).

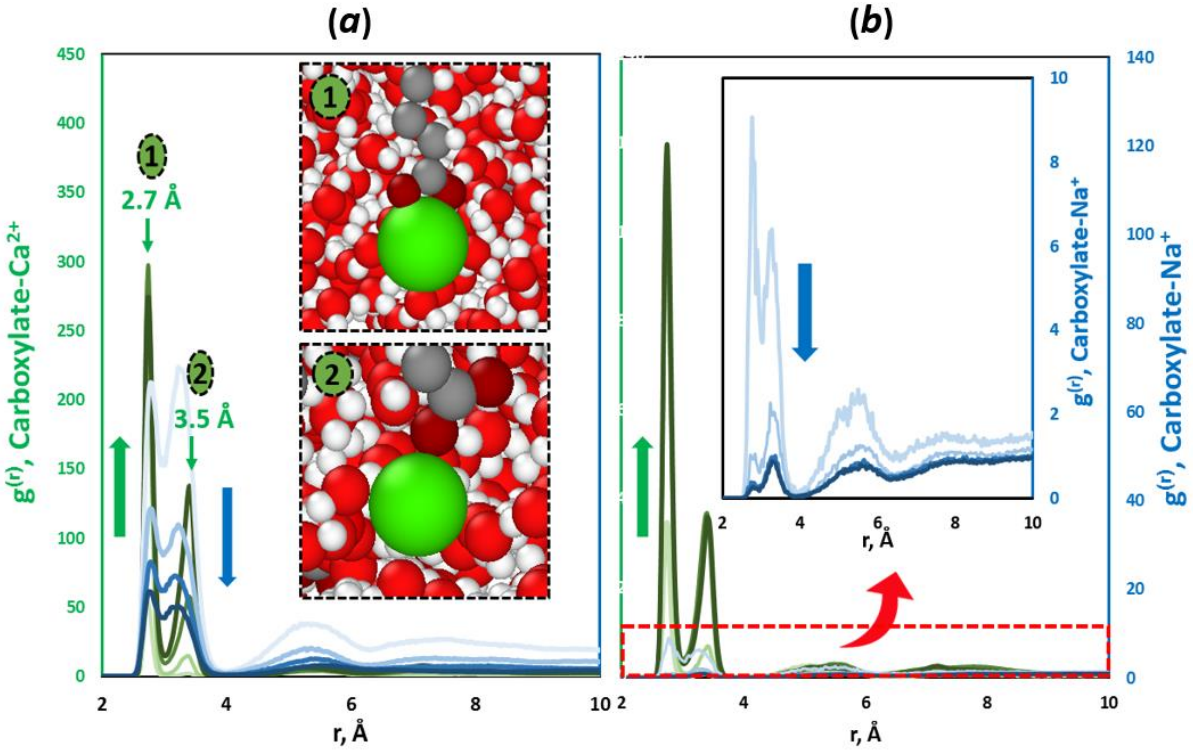

Figure 9 Radial distribution function, $g^{(r)}$, for carboxylate-Na^{+} (blue diagram) and carboxylate-Ca^{2+} (green diagram) interactions within the bottom (panel *a*), and top (panel *b*) interface regions upon using $CaCl_2$. Profiles were obtained using atomic trajectories collected at successive timespans, namely, 0-10 ns, 10-30 ns, 30-60 ns, and 60-100 ns, shown by light to thick diagrams, respectively. The peaks labeled in panel

(*a)* are due to: (1) bidentate, (2) monodentate, and (3) solvent-separated pairing of carboxylate-Ca^{2+}, as illustrated by corresponding insets. The domain delimited in panel *(b)* is closed up in the inset to show variations in carboxylate-Na^{+} RDF pertaining to upper interface zone. Blue and green arrows indicate the general (descending or ascending) trend of the carboxylate-Na^{+} and carboxylate-Ca^{2+} RDF profiles over time.

$MgCl_2$ solution

As shown in **Figure 2**, immersing the calcite-hydrocarbon system in an $MgCl_2$ solution is in many ways alike the $CaCl_2$ brine described above. In both cases, *in situ* interfacial sodium cations transferred to the soaking electrolyte solution, whereas divalent cations (Ca^{2+} or Mg^{2+}) approached toward the solid-brine interface, either surrounding the decanoate aggregate or residing in proximity to the calcite surface. Meanwhile, the originally ordered oil patch realigns through detachment of carboxylates, yielding a micelle-like structure with peripheral carboxylate groups. **Figure S6** shows the effectively time-invariant radius of gyration for treatment by $MgCl_2$ compared to that of $CaCl_2$, indicating less structural changes in the chunk of decanoate upon using the former solution.

Similar to the calcium ions, Mg^{2+} cations populate the region adjacent to the calcite slab, forming two adsorption layers at 5.2 and 7.1 Å (**Figure 10.b**). Generally speaking, divalent cations (Ca^{2+} or Mg^{2+}) diffusing from the soaking brine ($CaCl_2$ or $MgCl_2$) approach the calcite-water interface and, simultaneously, Na^{+} ions leave the calcite surface. This is basically an ion exchange process, where the *in situ* sodium ions were replaced by divalent cations. **Figure 8** shows the slower rate of such an exchange mechanism for $MgCl_2$ treatment (up to 60 ns) compared to the case of $CaCl_2$ (up to 40 ns). Compared to $CaCl_2$, **Figure S9** shows a slightly delayed appearance of carboxylates in the upper interface region. This comes with relatively lower level of carboxylate fraction observed by using $MgCl_2$ as well. The temporal variation of the fraction of Na^{+}, Cl^{-} and Ca^{2+}/Mg^{2+} ions seems comparably in both cases.

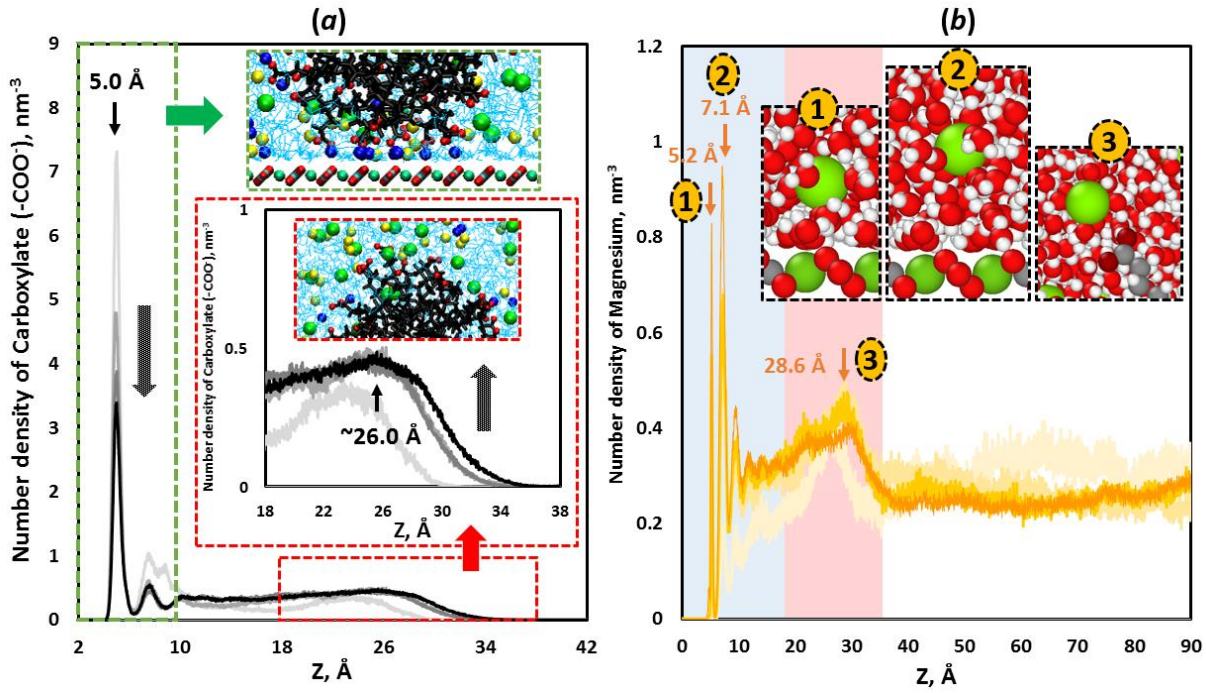

Figure 10 Number density distribution of (*a*) carboxylate, and (*b*) magnesium along the z-direction in case using $MgCl_2$. Light to dark diagrams belong to statistics collected at successive timespans: 0-10 ns, 10-30 ns, 30-60 ns, and 60-100 ns. Insets in panel (*a*) are the magnified image of the domains delimited within the dashed rectangles together with a schematic snapshot. Insets in panel (*b*) schematically illustrate the typical localization of Mg^{2+} cations in the corresponding adsorption layers. Areas highlighted in blue, red, and green in panel *b* correspond to the lower and upper interface regions, respectively. Black arrows show the general (descending or ascending) time-evolution trend of the carboxylate profiles at different regions.

Decanoate desorbed to greater extent when $CaCl_2$ brine was used, compared to when $MgCl_2$ was used (**Figure 6**). This can be explained by the stronger affinity of calcium cations for pairing with carboxylate groups, as inferred by different heights of carboxylate-Ca^{2+} and –Mg^{2+} RDF diagrams (**Figures 9.a** and **11.a,** respectively). It seems that carboxylate- Mg^{2+} interactions were not strong enough to overcome carboxylate-Na^{+} pairing in the proximity of the calcite surface. The differing complexion ability of Mg^{2+} and Ca^{2+} ions could be interpreted in terms of the stronger hydration of the former, as demonstrated by RDF profiles of Mg^{2+}- and Ca^{2+}-O_w (oxygen atom of water), shown in **Figure S12**. Magnesium solvation is so strong that solvent-separated ion pairs were formed by interaction of Mg^{2+} and $–COO^{-}$ entities (as illustrated in the inset of **Figure 11.a**).

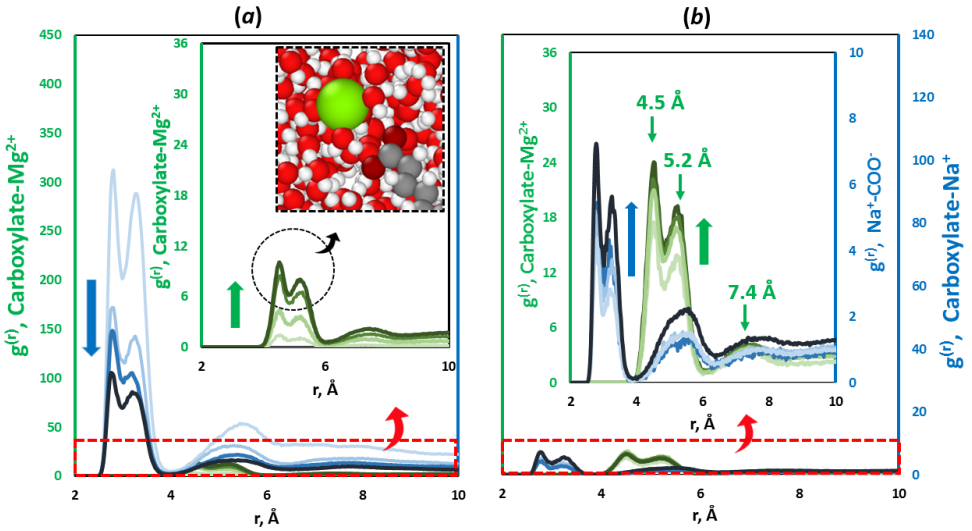

Figure 11 Radial distribution function, $g^{(r)}$, of carboxylate-Na^+ (blue diagram) and carboxylate-Mg^{2+} (green diagram) interaction upon using $MgCl_2$ within the bottom (panel *a*), and top (panel *b*) interface regions obtained at different timespans, namely, 0-10 ns, 10-30 ns, 30-60 ns, and 60-100 ns, shown by light to thick blue profiles, respectively. Domains enclosed in dashed rectangles are enlarged in corresponding insets. The peaks labeled in panel (*b)* are due to: (1) monodentate; (2) bidentate; and (3) solvent-separated pairing of carboxylate-Mg^{2+}. Arrows indicate the general time-evolution (descending or ascending) trend of the corresponding RDF profiles.

Similar to Ca^{2+} ions, Mg^{2+} cations tend to accumulate within the decanoate patch region (Z < ~36.0 Å) with higher concentration than the bulk space. However, unlike Ca^{2+}, **Figure 10.b** exhibits an uneven distribution of Mg^{2+} cations within the decanoate-occupied region, similar to the spatial distribution of carboxylates (**Figure 10.a**). The competing role of Na^+ and Mg^{2+} ions for pairing with carboxylates around the oil patch can be noted through the RDF profiles (**Figure 11.b**), as Na^+ and Mg^{2+} cations interacted comparably with the carboxylates within the upper part of the AOM. Altogether, the results reveal that Mg^{2+} is not as effective as Ca^{2+} cation for associating with carboxylates already paired to surface residing Na^+ cations.

Na_2SO_4 solution

Having explored the interfacial contribution and dynamics of Ca^{2+} and Mg^{2+} cations, we now aim to deepen our understanding of the role of sulfate, a prevalent divalent anion in natural

saline solutions. As before, realignment of decanoate molecules was observed upon contact with the Na_2SO_4 brine (**Figure 2**). It is interesting to note the accumulation of sulfate anions adjacent to the calcite surface, apparently by adhering to the resident sodium cations. This is quantitatively realized from the near-surface peaks in the distribution plots of SO_4^{2-} (**Figure 12)** and Na^+ (**Figure S13)** at 5.4 and 2.9 Å, respectively. The time-increasing Na^+-SO_4^{2-} RDF profile (**Figure S14**) further demonstrate the progressive linkage of the entering SO_4^{2-} anions to the Na^+ cations within the calcite neighborhood. 2D distribution plot (**Figure S15** in **Supporting Information**) clearly demonstrates the propensity of sulfates for preferentially localizing over sodium-occupied points over the calcite plane. Overall, surface Na^+ cations act as adsorption sites for bridging sulfate onto the calcite surface, as was observed for Cl^- ions.

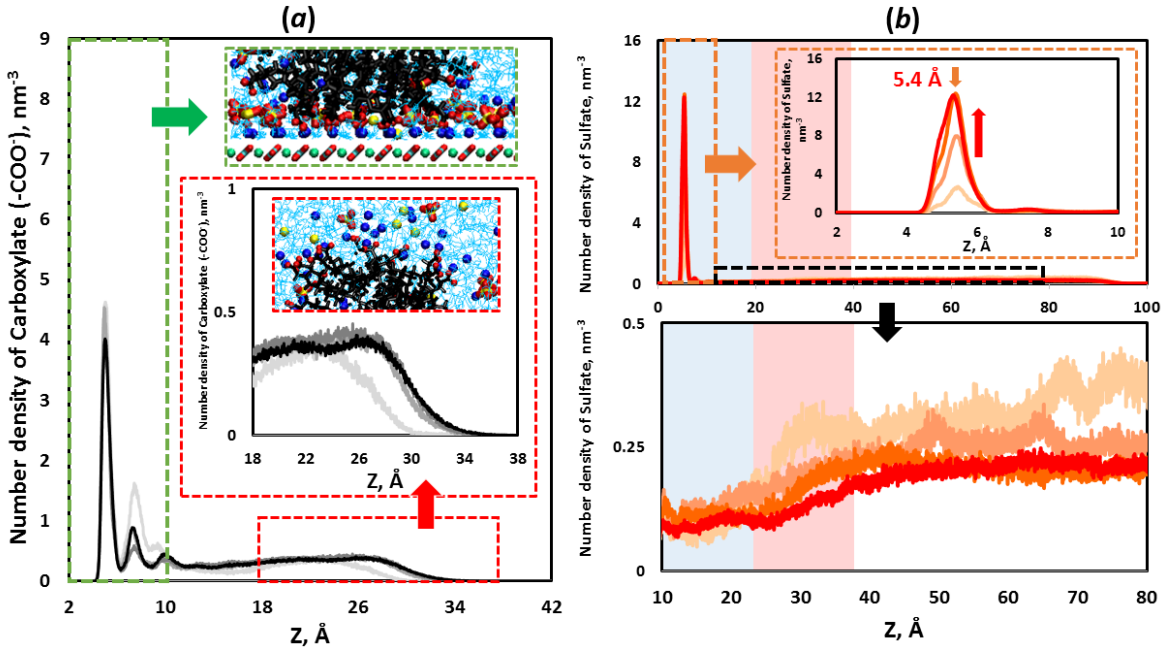

Figure 12 Number density profiles of (*a*) carboxylate, and (*b*) sulfate along the z-direction in case of Na_2SO_4. Light to dark diagrams belong to statistics collected at successive timespans: 0-10 ns, 10-30 ns, 30-60 ns, and 60-100 ns. Insets are the magnified image and schematic illustration of the domains delimited by dashed rectangles. Regions highlighted in blue and red in panel *b* correspond to lower and upper interfaces, respectively.

A small fraction of Na^+ cations (about 20%) left the calcite surface at the early 10.0 ns, as marked by the arrow in **Figure 8.** Afterwards, the mineral-brine interface gradually uptook excess sodium cations. The calcite plane accommodated sodium cations with a surface coverage of 19.5 nm^{-2}, 4 times greater than the value obtained by using DW (**Figure 6**). Meanwhile, sulfate anions steadily came to the calcite near-surface region, sitting over the pre-adsorbed Na^+ cations. The time-varying adsorption fraction profile of the sulfate correlates with that of the sodium cation, both achieving plateaus by the end of ~50.0 ns (**Figure 8**). Notably, the original Cl^- anions rapidly moved out of the calcite-water interface within the initial ~20.0 ns of the simulation (**Figure 8**). Excessive surface depletion of Cl^- ions (**Figure 6**) is caused possibly in response to the electrostatic repulsion induced by the invading sulfate anions. The surface repulsion of chloride anions leads to higher fraction of those ions within the upper interface regions, as inferred by **Figure S9**.

Compared to $MgCl_2$, $CaCl_2$ and even DW, a higher surface coverage of carboxylates was found when using the Na_2SO_4 solution, that is, 4.5 nm^{-2} (**Figures 6**). Interestingly, decanoate persisted at the surface when soaking the calcite slab in the Na_2SO_4 solution. The primary peak in **Figure 12.a** varied insignificantly, revealing a more robust, persistent linkage of carboxylate groups to the Na^+ layer covering the calcite surface. This is clearly reflected in the nearly invariant radius of gyration of oil clump over the simulation timeframe (**Figure S6**).

From **Figure 12.a**, decanoate detachment was mainly triggered by release of carboxylates contributing to the second density peak within the initial 30.0 ns. Thereafter, the fraction of carboxylates residing on the slab surface remained stable with minor fluctuations (**Figure 8**). This observation is in line with the delayed loading and minor instantaneous fluctuations of carboxylates at the upper interface region in comparison to other solutions, **Figure S9**. These together suggest a diminished instantaneous re-adsorption of decanoates, possibly in response to the negatively charged layer of sulfates developed over the calcite surface. Otherwise, we would expect the substantial re-attachment of decanoates to the Na^+ sites

covering the solid substrate. This is in line with the investigation of Bai et al., who noted the ability of sulfate to shield Na^+ sites on a $CaCO_3$ substrate, thus preventing adsorption of acetate molecules[58]. This deduction is also supported by the decreasing carboxylate-Na^+ RDF profile (**Figure S16**), clearly implying that such pairing does not extend near the calcite surface.

$MgSO_4$ solution

Thus far, the individual roles of Mg^{2+} and SO_4^{2-} ions in the evolution of a calcite-water interface containing a patch of adsorbed decanoate have separately been examined. Here, the joint contribution of those divalent ions is explored by considering the calcite slab immersed in $MgSO_4$ brine. In **Figure 2** the tendency of Mg^{2+} and SO_4^{2-} ions for associating within the $MgSO_4$ solution can be seen, and the resultant ionic pairs contact with the vertically upward decanoates. Meanwhile, the decanoate assembly reforms by release of carboxylates from the calcite plane, which is illustrated quantitatively in **Figure 13** as well. This pictorial evaluation is simply reflected to the anomalous time-variation of radius of gyration for decanoate clump, shown in **Figure S6**. The sudden increase of R_g within the early 20 ns, from initial value of ~ 8.0 Å to nearly 14.0 Å, results from the extra elongation of the decanoate molecules in response to the approaching ionic cluster, already illustrated in **Figure 2**.

The analyses demonstrated the appreciably greater surface concentration of sodium cation upon contact with $MgSO_4$ solution when compared to using the DW and $MgCl_2$ with the same total number of Na^+ ions *i.e.*, 7.3 against 4.0 and 4.3 nm^{-2} (**Figure 6**), respectively. Despite higher numbers of Na^+ sites existing on the calcite surface, the concentration of decanoate remaining over the calcite surface in the presence of $MgSO_4$ brine (2.4 nm^{-2}) is smaller than that was observed for the $MgCl_2$ or DW cases, 2.8 and 3.0 nm^{-2}, respectively (**Figure 6**). As with the Na_2SO_4 brine, some SO_4^{2-} anions diffuse towards the calcite-water interface, yielding a negatively-charged layer over the surface-lodging Na^+ cations, which is evident from the

sharp peaks in the density plots of sodium (**Figure S17**) and sulfates (**Figures 12.b**) at ~ 5.4 and ~2.9 Å, respectively. The increasing Na^{+}-SO_4^{2-} RDF diagram highlights the progressive linkage of the invading sulfate to the pre-adsorbed sodium cations. As such, Cl^{-} anions were substantially repelled from the calcite-brine interface region within the initial ~20.0 ns, down to ~20.0% of the initial surface concentration (**Figure 8**). In response to the presence of sulfate anions, the surface density of Cl^{-} ions after $MgSO_4$ treatment is markedly lower than when the $MgCl_2$ is used, 0.7 compared to 3.1 nm^{-2}, respectively (**Figure 6**).

The higher surface sorption of Mg^{2+} from the $MgSO_4$ solution (2.3 nm^{-2}) compared to the $MgCl_2$ brine (1.4 nm^{-2}), while both solutions carry the same amount of Mg^{2+}, *i.e.*, 1.0 $mol.dm^{-3}$ is worthy of further comment. This is counter-intuitive because the abundant sodium cations covering the calcite slab in the case of $MgSO_4$, would be expected to electrostatically repel Mg^{2+} ions from the calcite surface. Additionally, limited surface access of Mg^{2+} cations might be assumed because of involvement in the ionic pairs developed in the bulk $MgSO_4$ solution.

Despite these inhibiting factors, Mg^{2+} cations were attracted to the calcite surface by the negatively charged layer developed by the adsorbed sulfates. The magnesium-sulfate RDF profile and the accompanying snapshot (**Figure S18**) indicated the SO_4^{2-}-mediated sorption of Mg^{2+} cations to the surface-covering Na^{+} ions, as if a sulfate was shared and bridged between a magnesium and a sodium cation. **Figure 8** shows the simultaneous buildup of sulfate and magnesium ions over the substrate by the end of ~60.0 ns to achieve nearly equal surface concentrations that is 3.0 and 2.8 nm^{-2} (**Figure 6**), respectively. Analogously, **Figure S9** exhibits simultaneous accumulation of Mg^{2+} and SO_4^{2-} ions within the upper interface region.

In brief, we recognize the assisting role of SO_4^{2-} anions for drawing Mg^{2+} cations closer to the calcite surface and, subsequently, having a greater chance for associating with the carboxylate groups. This is simply inferred from the stronger interaction of carboxylate-Mg^{2+} near the calcite surface in the presence of $MgSO_4$ (**Figure S19**), compared to when using

$MgCl_2$ (**Figure 11**). This explains the larger desorption of decanoates upon contacting the calcite interface with $MgSO_4$ solution compared to that for $MgCl_2$ solution (**Figure 6**).

The hump-shaped concentration diagrams of Mg^{2+} and SO_4^{2-} (**Figures 13.b-c**) reflects the inhomogeneous distribution of those ions as a result of association within the immersing solution. That hump steadily moves downwards to finally stay at ~ 35.0 Å, where the $MgSO_4^0$ pairs touching the decanoates. In a closer look, we notice the early-time accumulation of Mg^{2+} cations over the surface sorbed decanoate, indicated by a small arrow in **Figure 13.b.** Because of that microscopic localization of ions, the hydrocarbon-contaminated calcite substrate would behave as a hydrophilic environment.

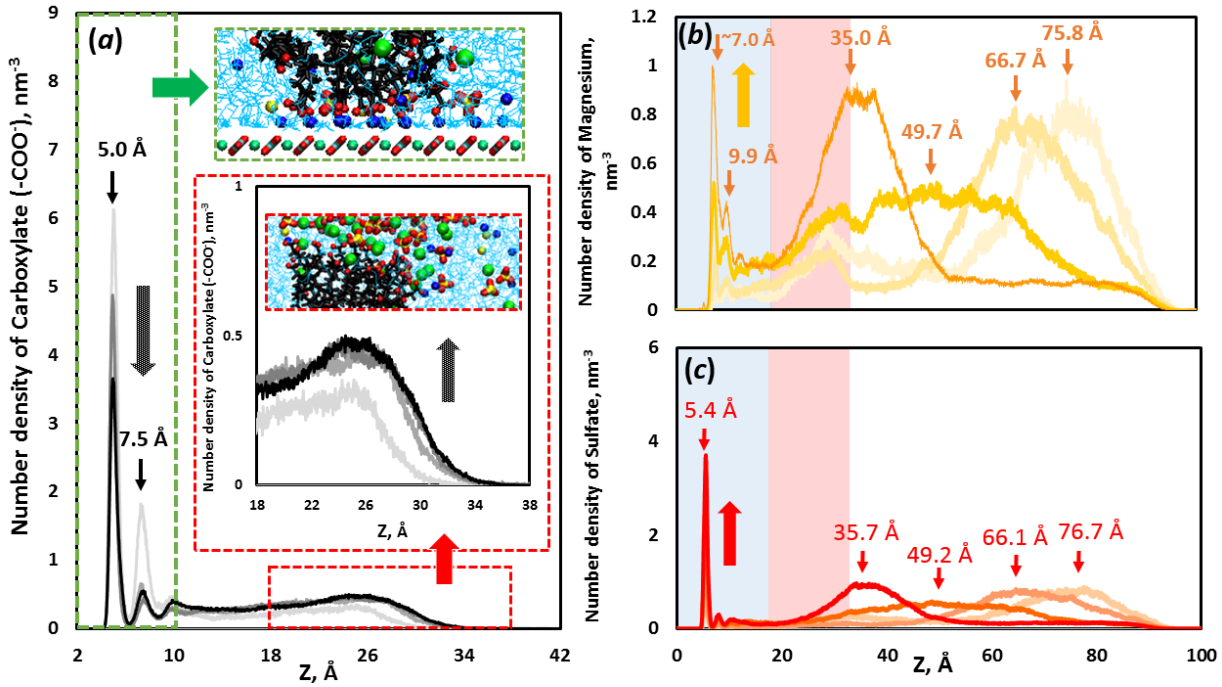

Figure 13 Number density distribution of (*a*) carboxylate, (*b*) magnesium, and (c) sulfate along the z-direction in case of $MgSO_4$. Light to dark diagrams belong to statistics collected at successive timespans: 0-10 ns, 10-30 ns, 30-60 ns, and 60-100 ns. Insets in panel (*a*) are the magnified image and schematic illustration of the domains delimited by dashed rectangles. The red arrow in panel (b) indicates the loading of Mg^{2+} over the oil assembly at the preliminary stage of the process. Regions highlighted in blue and red, correspond to lower and upper interfaces, respectively. Arrows indicate the general time-evolution (descending or ascending) trend of the corresponding profiles.

Discussion

In all cases of contacting the calcite interface to an electrolyte solution, a micelle-shape patch of decanoates develops by realignment of those molecules. As such, a charged interface appears around (especially at the top of) the oil patch made up of outward carboxylate terminal groups contacting the soaking brine solution. A similar change was observed by Lowry et al., who applied MD simulation to examine structural evolution of a model oil (a mixture of asphaltenes and naphthenic acids) adsorbed on a limestone slab [59]. In effect, interfacial organic matter (hydrocarbon deposits or contaminants) covering the pore walls of reservoir rocks, can be imagined as charged sites even enhancing hydrophilicity of the basal mineral substrate. This is supported by nanoscopic experiments with AFM performed by Hassenkam and co-workers, who pointed out that tightly adsorbed hydrocarbons majorly contribute to the overall ion-specific wetting character of the natural rocks [16,34,60]. The presence of AOM leads to the complex response of natural oil-bearing rock samples to changing ionic composition of the surrounding aqueous environment. As a result, zeta potential measurements by Jackson and co-workers showed a wide spectrum of surface charges for natural carbonates [61–63], possibly due to the existence of organic impurities contained in the pore structure of those rocks. Altogether, the overall surface characteristics of an oil-bearing carbonate substrate is not solely controlled by the bare (intact) rock-water interface [64–66]; rather, we should think of the combined effect of the mineral surface and sporadic organic sites.

Consistent with former investigations [23,67], the importance of the positively-charged Na^+ layer developed over a calcite plane as preferential adsorption sites for attracting anions and carboxylate head-groups, and binding them to the surface has been also observed in the present study. It should be emphasized that adsorption and localization of sodium cations on the $CaCO_3$ surface is in agreement with the nanoscopic experimental study by Ricci et al., who directly visualized the residence of Na^+ cations immediate to a calcite-solution interface

[38]. Therefore, any factor triggering surface removal of Na^+ cations would disturb the near-surface distribution of other ions as well, leading to the detachment of carboxylates and consequently, conformational variation of the surface bound oil. It could happen as a result of dilution of the mineral-brine interface, as observed earlier upon treating the oil-bearing calcite using DW. This provides a likely interpretation for the enhancement in the water-wet affinity of carbonates upon soaking or flushing by low-salinity brines. The experimental study conducted by Shaik et al. showed that reducing the amount of Na^+ ions favors desorption of naphthenic acids from a calcite surface [27]. On the other hand, reducing surface residing sodium cations promotes the chance of divalent cations, Ca^{2+} and Mg^{2+}, to come close to the calcite plane and possibly associating with carboxylate groups [68].

Our results demonstrate the ability of divalent cations for promoting release of carboxylate compounds from a calcite plane. We noticed that the interface contacted by $CaCl_2$ brine experienced enhanced desorption of decanoate to a greater extent than when solely using DW. Therefore, in a macroscopic limit, treatment by a Ca^{2+}-rich saline solutions shifts affinity of a calcite surface to water-favoring state as frequently reported in previous conventional laboratory tests [69]. This effect has been confirmed by force spectroscopy technique in a recent study by Ding et al. as well [70]. They measured the interaction force of an oil droplet from a calcite surface and noticed the tendency of Ca^{2+} cations for mitigating attraction force in a NaCl solution. In a well-known multi-component ions exchange mechanism, proposed by Austad and co-workers [69,71,72], divalent cations tend to coordinate the negatively-charged moieties (typically carboxylate) of polar organic molecules, thus facilitating the desorption of those compounds from a calcite surface, which was verified in the present study at atomic/molecular level. Of particular interest, the relative merit of Ca^{2+} over Mg^{2+} in competing with Na^+ cations for complexion with carboxylate head-groups was observed. In comparison to the calcium ion, the smaller Mg^{2+} cation holds a tight hydration shell, hindering its chance to approach the calcite surface and the chance for pairing with carboxylate head-groups. The

water-mediated complexation of Mg^{2+}-carboxylate has been attributed to the unfavorable energy penalty to be incurred for disrupting the ions' hydration shell [58].

The present results revealed the strong propensity of sulfates for coordinating the surface-lodging Na^{+} cations and effectively developing a negatively-charged layer over the calcite surface. This phenomenon has been mirrored in former studies to negative surface potential of $CaCO_3$ exposed to SO_4^{2-}-rich solutions [62]. Such sulfate layer is able to repel free carboxylate compounds, thereby diminishing their chance of re-attachment. Gomari et al. suggested this mechanism upon observing ion-sensitive capacity of calcite substrates for adsorbing fatty acids [73]. The authors stated that sulfate adsorption modifies a $CaCO_3$ plane, giving negative charge and diminishes the available Na^{+} sites for capturing carboxylic compounds. In a CFM investigation by Ding et al., they reported the repulsive interaction between an oil droplet and calcite surface in Na_2SO_4 solution [70].

Sulfate adsorption provides favorable sites for drawing Mg^{2+} to the calcite surface. By using $MgSO_4$, we found the Mg^{2+}/SO_4^{2-} combination is more effective in releasing carboxylate groups than having those ions alone, *i.e.*, using either $MgCl_2$ or Na_2SO_4. This molecular observation is in accord with a majority of prior researches mentioning the catalytic role of sulfate anions in the context of improving the probability of Mg^{2+} cations for visiting the calcite-water interface and releasing Na-bridged carboxylates from the solid surface [4]. Following the work of Bai et al. and Koleini et al. [23,58], one could assume the extent of decanoate adsorption as a measure of surface wettability, *i.e.*, being more oil-wet at greater surface coverage by carboxylates. With this consideration, our computational results are in accord with former experimental investigations in which the assisting contribution of sulfates has been frequently presumed for interpreting the wettability alteration of carbonates upon treatment by sulfate-rich brines [74].

Concluding remarks

This research is a step towards understanding nanoscopic interactions underlying ion-engineered waterflooding of carbonate reservoirs. In this research, a series of atomistic simulations were performed to advance our molecular-level understanding of the behavior of major constituting ions of natural saline solutions (Na^+, Cl^-, Ca^{2+}, Mg^{2+}, and SO_4^{2-}) in the vicinity of a decanoate-contaminated calcite surface. The results highlight the importance of originally adsorbed hydrocarbons in regulating the ionic composition adjacent to a calcite substrate. In keep with former laboratory experiments, we believe the overall interfacial behavior of natural (oil-bearing) carbonates is governed both by the mineral surface chemistry and also the residing charged sites of polar hydrocarbons.

The key role of Na^+ cations in linking negatively-charged head-groups, here carboxylates, onto a $CaCO_3$ surface was noted. Any factor triggering the breakage of Na^+-shared carbonate-carboxylate pairing would lead to the release of polar molecules from the calcite surface. This process is promoted in the presence of divalent cations (Ca^{2+} or Mg^{2+}), having a strong affinity for coordinating the carboxylate functional groups and releasing them from the calcite surface. However, because of being densely hydrated, Mg^{2+} ions were less effective than Ca^{2+} in promoting desorption. Consistent with experimental observations, we observed the assisting role of sulfate for improving interfacial binding of magnesium cations. Furthermore, sulfate showed a strong affinity for developing a negatively-charged layer over a calcite plane by attaching to the surface-covering Na^+ cations. This could inhibit the re-adsorption of polar molecules. It is anticipated that the atomistic insights gained in this study will help rational design of waterflooding operations as well as geochemical processes like soil remediation, NAPL removal from underground aquifers, and geological storage of hazardous gases.

ASSOCIATED CONTENT

Supporting Information

The Supporting Information is available free of charge on the ACS Publications website at DOI:

Evaluating adequacy of the simulation timeframes; list of force-field parameters employed for MD simulation; radius of gyration; distribution profile of methyl groups (-CH_3); MSD of ions at different solutions; time-varying fraction of ions and carboxylates detected within the lower interface region in case of using DW; time-varying fraction of ions and carboxylates detected within the upper interface; and distribution diagrams and RDF profiles.

AUTHOR INFORMATION

Corresponding Author

***Email:** shahab@sharif.edu & dr.ayatollahi@gmail.com

ORCID

Mohammad Hasan Badizad: 0000-0001-8144-6896

Mohammad Mehdi Koleini: 0000-0001-7950-951X

Hugh Christopher Greenwell: 0000-0001-5719-8415

Shahab Ayatollahi: 0000-0001-7561-6393

Mohammad Hossein Ghazanfari: 0000-0001-7512-8728

Notes

The authors declare no competing financial interest.

References

(1) Mahani, H.; Keya, A. L.; Berg, S.; Bartels, W.-B.; Nasralla, R.; Rossen, W. R. Insights into the Mechanism of Wettability Alteration by Low-Salinity Flooding (LSF) in Carbonates. *Energy & Fuels* **2015**, *29* (3), 1352–1367. https://doi.org/10.1021/ef5023847.

(2) Mohammadi, S.; Mahani, H.; Ayatollahi, S.; Niasar, V. Impact of Oil Polarity on the Mixing Time at the Pore Scale in Low Salinity Waterflooding. *Energy and Fuels* **2020**. https://doi.org/10.1021/acs.energyfuels.0c01972.

(3) Haghtalab, A.; Badizad, M. H. Solubility of Gypsum in Aqueous NaCl + K2SO4 Solution Using Calcium Ion Selective Electrode-Investigation of Ionic Interactions. *Fluid Phase Equilib.* **2016**. https://doi.org/10.1016/j.fluid.2015.10.011.

(4) Rashid, S.; Mousapour, M. S.; Ayatollahi, S.; Vossoughi, M.; Beigy, A. H. Wettability Alteration in Carbonates during “Smart Waterflood”: Underling Mechanisms and the Effect of Individual Ions. *Colloids Surfaces A Physicochem. Eng. Asp.* **2015**. https://doi.org/10.1016/j.colsurfa.2015.09.067.

(5) Mahani, H.; Menezes, R.; Berg, S.; Fadili, A.; Nasralla, R.; Voskov, D.; Joekar-Niasar, V. Insights into the Impact of Temperature on the Wettability Alteration by Low Salinity in Carbonate Rocks. *Energy and Fuels* **2017**. https://doi.org/10.1021/acs.energyfuels.7b00776.

(6) Koleini, M. M.; Badizad, M. H.; Mahani, H.; Dastjerdi, A. M.; Ayatollahi, S.; Ghazanfari, M. H. Atomistic Insight into Salinity Dependent Preferential Binding of Polar Aromatics to Calcite/Brine Interface: Implications to Low Salinity Waterflooding. *Sci. Rep.* **2021**. https://doi.org/10.1038/s41598-021-91402-0.

(7) Badizad, M. H.; Koleini, M. M.; Hartkamp, R.; Ayatollahi, S.; Ghazanfari, M. H. How

Do Ions Contribute to Brine-Hydrophobic Hydrocarbon Interfaces? An in Silico Study. *J. Colloid Interface Sci.* **2020**. https://doi.org/10.1016/j.jcis.2020.04.060.

(8) Badizad, M. H.; Koleini, M. M.; Greenwell, H. C.; Ayatollahi, S.; Ghazanfari, M. H.; Mohammadi, M. Ion-Specific Interactions at Calcite-Brine Interfaces: A Nano-Scale Study of the Surface Charge Development and Preferential Binding of Polar Hydrocarbons. *Phys. Chem. Chem. Phys.* **2020**. https://doi.org/10.1039/d0cp04828c.

(9) Koleini, M. M.; Badizad, M. H.; Kargozarfard, Z.; Ayatollahi, S. The Impact of Salinity on Ionic Characteristics of Thin Brine Film Wetting Carbonate Minerals: An Atomistic Insight. *Colloids Surfaces A Physicochem. Eng. Asp.* **2019**, *571*, 27–35. https://doi.org/10.1016/j.colsurfa.2019.03.070.

(10) Keller, K. S.; Olsson, M. H. M.; Yang, M.; Stipp, S. L. S. Adsorption of Ethanol and Water on Calcite: Dependence on Surface Geometry and Effect on Surface Behavior. *Langmuir* **2015**, *31* (13), 3847–3853. https://doi.org/10.1021/la504319z.

(11) Zhang, P.; Tweheyo, M. T.; Austad, T. Wettability Alteration and Improved Oil Recovery by Spontaneous Imbibition of Seawater into Chalk: Impact of the Potential Determining Ions Ca2+, Mg2+, and SO42-. *Colloids Surfaces A Physicochem. Eng. Asp.* **2007**, *301* (1–3), 199–208. https://doi.org/10.1016/j.colsurfa.2006.12.058.

(12) Das, S.; Nguyen, Q.; Patil, P. D.; Yu, W.; Bonnecaze, R. T. Wettability Alteration of Calcite by Nonionic Surfactants. *Langmuir* **2018**. https://doi.org/10.1021/acs.langmuir.8b02098.

(13) Lu, Y.; Najafabadi, N. F.; Firoozabadi, A. Effect of Low-Concentration of 1-Pentanol on the Wettability of Petroleum Fluid-Brine-Rock Systems. *Langmuir* **2019**. https://doi.org/10.1021/acs.langmuir.9b00099.

(14) Rios-Carvajal, T.; Pedersen, N. R.; Bovet, N.; Stipp, S. L. S.; Hassenkam, T. Specific

Ion Effects on the Interaction of Hydrophobic and Hydrophilic Self-Assembled Monolayers. *Langmuir* **2018**, *34* (35), 10254–10261.

(15) Pedersen, N. R.; Hassenkam, T.; Ceccato, M.; Dalby, K. N.; Mogensen, K.; Stipp, S. L. S. Low Salinity Effect at Pore Scale: Probing Wettability Changes in Middle East Limestone. *Energy and Fuels* **2016**. https://doi.org/10.1021/acs.energyfuels.5b02562.

(16) Matthiesen, J.; Hassenkam, T.; Bovet, N.; Dalby, K. N.; Stipp, S. L. S. Adsorbed Organic Material and Its Control on Wettability. *Energy and Fuels* **2017**. https://doi.org/10.1021/acs.energyfuels.6b00627.

(17) Koleini, M. M.; Badizad, M. H.; Ayatollahi, S. An Atomistic Insight into Interfacial Properties of Brine Nanofilm Confined between Calcite Substrate and Hydrocarbon Layer. *Appl. Surf. Sci.* **2019**, *490*, 89–101. https://doi.org/10.1016/j.apsusc.2019.05.337.

(18) Dehaghani, A. H. S.; Taleghani, M. S.; Badizad, M. H.; Daneshfar, R. Simulation Study of the Gachsaran Asphaltene Behavior within the Interface of Oil/Water Emulsion: A Case Study. *Colloids Interface Sci. Commun.* **2019**. https://doi.org/10.1016/j.colcom.2019.100202.

(19) Underwood, T.; Erastova, V.; Cubillas, P.; Greenwell, H. C. Molecular Dynamic Simulations of Montmorillonite Organic Interactions under Varying Salinity: An Insight into Enhanced Oil Recovery. *J. Phys. Chem. C* **2015**. https://doi.org/10.1021/acs.jpcc.5b00555.

(20) Underwood, T.; Erastova, V.; Greenwell, H. C. Wetting Effects and Molecular Adsorption at Hydrated Kaolinite Clay Mineral Surfaces. *J. Phys. Chem. C* **2016**. https://doi.org/10.1021/acs.jpcc.6b00187.

(21) Zhao, J.; Yao, G.; Ramisetti, S. B.; Hammond, R. B.; Wen, D. Molecular Dynamics

Investigation of Substrate Wettability Alteration and Oil Transport in a Calcite Nanopore. *Fuel* **2019**. https://doi.org/10.1016/j.fuel.2018.11.089.

(22) Zhao, J.; Yao, G.; Wen, D. Salinity-Dependent Alterations of Static and Dynamic Contact Angles in Oil/Brine/Calcite Systems: A Molecular Dynamics Simulation Study. *Fuel* **2020**. https://doi.org/10.1016/j.fuel.2020.117615.

(23) Koleini, M. M.; Badizad, M. H.; Hartkamp, R.; Ayatollahi, S.; Ghazanfari, M. H. The Impact of Salinity on the Interfacial Structuring of an Aromatic Acid at the Calcite/Brine Interface: An Atomistic View on Low Salinity Effect. *J. Phys. Chem. B* **2020**, *124* (1), 224–233. https://doi.org/10.1021/acs.jpcb.9b06987.

(24) Koleini, M. M.; Badizad, M. H.; Kargozarfard, Z.; Ayatollahi, S. Interactions between Rock/Brine and Oil/Brine Interfaces within Thin Brine Film Wetting Carbonates: A Molecular Dynamics Simulation Study. *Energy & Fuels* **2019**, *33* (9), 7983–7992. https://doi.org/10.1021/acs.energyfuels.9b00496.

(25) Koleini, M. M.; Mehraban, M. F.; Ayatollahi, S. Effects of Low Salinity Water on Calcite/Brine Interface: A Molecular Dynamics Simulation Study. *Colloids Surfaces A Physicochem. Eng. Asp.* **2018**, *537*, 61–68.

(26) Song, J.; Wang, Q.; Shaik, I.; Puerto, M.; Bikkina, P.; Aichele, C.; Biswal, S. L.; Hirasaki, G. J. Effect of Salinity, Mg2+ and SO42− on “Smart Water”-Induced Carbonate Wettability Alteration in a Model Oil System. *J. Colloid Interface Sci.* **2020**. https://doi.org/10.1016/j.jcis.2019.12.040.

(27) Shaik, I. K.; Song, J.; Biswal, S. L.; Hirasaki, G. J.; Bikkina, P. K.; Aichele, C. P. Effect of Brine Type and Ionic Strength on the Wettability Alteration of Naphthenic-Acid-Adsorbed Calcite Surfaces. *J. Pet. Sci. Eng.* **2020**. https://doi.org/10.1016/j.petrol.2019.106567.

(28) Seiedi, O.; Rahbar, M.; Nabipour, M.; Emadi, M. A.; Ghatee, M. H.; Ayatollahi, S. Atomic Force Microscopy (AFM) Investigation on the Surfactant Wettability Alteration Mechanism of Aged Mica Mineral Surfaces. *Energy and Fuels* **2011**. https://doi.org/10.1021/ef100699t.

(29) Strand, S.; Puntervold, T.; Austad, T. Water Based EOR from Clastic Oil Reservoirs by Wettability Alteration: A Review of Chemical Aspects. *J. Pet. Sci. Eng.* **2016**. https://doi.org/10.1016/j.petrol.2016.08.012.

(30) Hu, X.; Yutkin, M. P.; Hassan, S.; Wu, J.; Prausnitz, J. M.; Radke, C. J. Asphaltene Adsorption from Toluene onto Silica through Thin Water Layers. *Langmuir* **2019**. https://doi.org/10.1021/acs.langmuir.8b03835.

(31) Sand, K. K.; Yang, M.; Makovicky, E.; Cooke, D. J.; Hassenkam, T.; Bechgaard, K.; Stipp, S. L. S. Binding of Ethanol on Calcite: The Role of the OH Bond and Its Relevance to Biomineralization. *Langmuir : the ACS journal of surfaces and colloids*. 2010, pp 15239–15247. https://doi.org/10.1021/la101136j.

(32) Lorenz, B.; Ceccato, M.; Andersson, M. P.; Dobberschütz, S.; Rodriguez-Blanco, J. D.; Dalby, K. N.; Hassenkam, T.; Stipp, S. L. S. Salinity-Dependent Adhesion Response Properties of Aluminosilicate (K-Feldspar) Surfaces. *Energy and Fuels* **2017**. https://doi.org/10.1021/acs.energyfuels.6b02969.

(33) Liu, Z. L.; Rios-Carvajal, T.; Andersson, M. P.; Ceccato, M.; Stipp, S. L. S.; Hassenkam, T. Insights into the Pore-Scale Mechanism for the Low-Salinity Effect: Implications for Enhanced Oil Recovery. *Energy & Fuels* **2018**, *32* (12), 12081–12090.

(34) Hassenkam, T.; Skovbjerg, L. L.; Stipp, S. L. S. Probing the Intrinsically Oil-Wet Surfaces of Pores in North Sea Chalk at Subpore Resolution. *Proc. Natl. Acad. Sci. U. S. A.* **2009**. https://doi.org/10.1073/pnas.0901051106.

(35) Downs, R. T.; Hall-Wallace, M. The American Mineralogist Crystal Structure Database. *Am. Mineral.* **2003**. https://doi.org/10.5860/choice.43sup-0302.

(36) Frenkel, D.; Smit, B.; Ratner, M. A. Understanding Molecular Simulation: From Algorithms to Applications. *Phys. Today* **1997**, *50* (7), 66–66. https://doi.org/10.1063/1.881812.

(37) Badizad, M. H.; Koleini, M. M.; Greenwell, H. C.; Ayatollahi, S.; Ghazanfari, M. H. A Deep Look into the Dynamics of Saltwater Imbibition in a Calcite Nanochannel: Temperature Impacts Capillarity Regimes. *Langmuir* **2020**. https://doi.org/10.1021/acs.langmuir.0c00437.

(38) Ricci, M.; Spijker, P.; Stellacci, F.; Molinari, J.-F.; Voïtchovsky, K. Direct Visualization of Single Ions in the Stern Layer of Calcite. *Langmuir* **2013**, *29* (7), 2207–2216. https://doi.org/10.1021/la3044736.

(39) Saeedi Dehaghani, A. H.; Badizad, M. H. Impact of Ionic Composition on Modulating Wetting Preference of Calcite Surface: Implication for Chemically Tuned Water Flooding. *Colloids Surfaces A Physicochem. Eng. Asp.* **2019**. https://doi.org/10.1016/j.colsurfa.2019.02.009.

(40) Wu, Y.; Shuler, P. J.; Blanco, M.; Tang, Y.; Goddard, W. A. An Experimental Study of Wetting Behavior and Surfactant EOR in Carbonates with Model Compounds. *SPE J.* **2008**. https://doi.org/10.2118/99612-PA.

(41) Juhl, K. M. S.; Pedersen, C. S.; Bovet, N.; Dalby, K. N.; Hassenkam, T.; Andersson, M. P.; Okhrimenko, D.; Stipp, S. L. S. Adhesion of Alkane as a Functional Group on Muscovite and Quartz: Dependence on PH and Contact Time. *Langmuir* **2014**. https://doi.org/10.1021/la5024967.

(42) Chen, Y.; Ubaidah, A.; Elakneswaran, Y.; Niasar, V. J.; Xie, Q. Detecting PH and

Ca2+ Increase during Low Salinity Waterflooding in Carbonate Reservoirs: Implications for Wettability Alteration Process. *J. Mol. Liq.* **2020**. https://doi.org/10.1016/j.molliq.2020.114003.

(43) Wellen, B. A.; Lach, E. A.; Allen, H. C. Surface p: K a of Octanoic, Nonanoic, and Decanoic Fatty Acids at the Air-Water Interface: Applications to Atmospheric Aerosol Chemistry. *Phys. Chem. Chem. Phys.* **2017**. https://doi.org/10.1039/c7cp04527a.

(44) Thompson, D. W.; Pownall, P. G. Surface Electrical Properties of Calcite. *J. Colloid Interface Sci.* **1989**, *131* (1), 74–82. https://doi.org/10.1016/0021-9797(89)90147-1.

(45) Fang, T.; Wang, M.; Li, J.; Liu, B.; Shen, Y.; Yan, Y.; Zhang, J. Study on the Asphaltene Precipitation in CO2 Flooding: A Perspective from Molecular Dynamics Simulation. *Ind. Eng. Chem. Res.* **2018**. https://doi.org/10.1021/acs.iecr.7b03700.

(46) Haagh, M. E. J.; Siretanu, I.; Duits, M. H. G.; Mugele, F. Salinity-Dependent Contact Angle Alteration in Oil/Brine/Silicate Systems: The Critical Role of Divalent Cations. *Langmuir* **2017**. https://doi.org/10.1021/acs.langmuir.6b04470.

(47) Martínez, L.; Andrade, R.; Birgin, E. G.; Martínez, J. M. PACKMOL: A Package for Building Initial Configurations for Molecular Dynamics Simulations. *J. Comput. Chem.* **2009**, *30* (13), 2157–2164. https://doi.org/10.1002/jcc.21224.

(48) Plimpton, S.; Crozier, P.; Thompson, A. LAMMPS-Large-Scale Atomic/Molecular Massively Parallel Simulator. *Sandia Natl. Lab.* **2007**.

(49) Xiao, S.; Edwards, S. A.; Gräter, F. A New Transferable Force-Field for Simulating the Mechanics of CaCO3 Crystals. *J. Phys. Chem. C* **2011**, *115* (41), 20067–20075. https://doi.org/10.1021/jp202743v.

(50) Wang, S.; Feng, Q.; Javadpour, F.; Yang, Y. B. Breakdown of Fast Mass Transport of Methane through Calcite Nanopores. *J. Phys. Chem. C* **2016**.

https://doi.org/10.1021/acs.jpcc.6b05511.

(51) Bruno, M.; Massaro, F. R.; Pastero, L.; Costa, E.; Rubbo, M.; Prencipe, M.; Aquilano, D. New Estimates of the Free Energy of Calcite/Water Interfaces for Evaluating the Equilibrium Shape and Nucleation Mechanisms. *Cryst. Growth Des.* **2013**. https://doi.org/10.1021/cg3015817.

(52) Santos, M. S.; Franco, L. F. M.; Castier, M.; Economou, I. G. Molecular Dynamics Simulation of n -Alkanes and CO 2 Confined by Calcite Nanopores. *Energy & Fuels* **2018**, *32* (2), 1934–1941. https://doi.org/10.1021/acs.energyfuels.7b02451.

(53) Damm, W.; Frontera, A.; Tirado--Rives, J.; Jorgensen, W. L. OPLS All-Atom Force Field for Carbohydrates. *J. Comput. Chem.* **1997**, *18* (16), 1955–1970.

(54) Eslami, H.; Khani, M.; Müller-Plathe, F. Gaussian Charge Distributions for Incorporation of Electrostatic Interactions in Dissipative Particle Dynamics: Application to Self-Assembly of Surfactants. *J. Chem. Theory Comput.* **2019**. https://doi.org/10.1021/acs.jctc.9b00174.

(55) Afandak, A.; Eslami, H. Ion-Pairing and Electrical Conductivity in the Ionic Liquid 1-n-Butyl-3-Methylimidazolium Methylsulfate [Bmim][MeSO4]: Molecular Dynamics Simulation Study. *J. Phys. Chem. B* **2017**. https://doi.org/10.1021/acs.jpcb.7b06039.

(56) Eslami, H.; Müller-Plathe, F. How Thick Is the Interphase in an Ultrathin Polymer Film? Coarse-Grained Molecular Dynamics Simulations of Polyamide-6,6 on Graphene. *J. Phys. Chem. C* **2013**. https://doi.org/10.1021/jp400142h.

(57) Koleini, M. M.; Badizad, M. H.; Ghatee, M. H.; Ayatollahi, S. An Atomistic Insight into the Implications of Ion-Tuned Water Injection in Wetting Preferences of Carbonate Reservoirs. *J. Mol. Liq.* **2019**. https://doi.org/10.1016/j.molliq.2019.111530.

(58) Bai, S.; Kubelka, J.; Piri, M. A Positively Charged Calcite Surface Model for Molecular

Dynamics Studies of Wettability Alteration. *J. Colloid Interface Sci.* **2020**. https://doi.org/10.1016/j.jcis.2020.02.037.

(59) Lowry, E.; Sedghi, M.; Goual, L. Molecular Simulations of NAPL Removal from Mineral Surfaces Using Microemulsions and Surfactants. *Colloids Surfaces A Physicochem. Eng. Asp.* **2016**. https://doi.org/10.1016/j.colsurfa.2016.07.002.

(60) Matthiesen, J.; Bovet, N.; Hilner, E.; Andersson, M. P.; Schmidt, D. A.; Webb, K. J.; Dalby, K. N.; Hassenkam, T.; Crouch, J.; Collins, I. R.; et al. How Naturally Adsorbed Material on Minerals Affects Low Salinity Enhanced Oil Recovery. *Energy and Fuels* **2014**. https://doi.org/10.1021/ef500218x.

(61) Alroudhan, A.; Vinogradov, J.; Jackson, M. D. Zeta Potential of Intact Natural Limestone: Impact of Potential-Determining Ions Ca, Mg and SO4. *Colloids Surfaces A Physicochem. Eng. Asp.* **2016**, *493*, 83–98. https://doi.org/10.1016/j.colsurfa.2015.11.068.

(62) Al Mahrouqi, D.; Vinogradov, J.; Jackson, M. D. Zeta Potential of Artificial and Natural Calcite in Aqueous Solution. *Advances in Colloid and Interface Science*. 2017, pp 60–76. https://doi.org/10.1016/j.cis.2016.12.006.

(63) Jackson, M. D.; Al-Mahrouqi, D.; Vinogradov, J. Zeta Potential in Oil-Water-Carbonate Systems and Its Impact on Oil Recovery during Controlled Salinity Water-Flooding. *Sci. Rep.* **2016**, *6*, 37363. https://doi.org/10.1038/srep37363.

(64) Ding, H.; Rahman, S. Experimental and Theoretical Study of Wettability Alteration during Low Salinity Water Flooding-an State of the Art Review. *Colloids and Surfaces A: Physicochemical and Engineering Aspects*. 2017. https://doi.org/10.1016/j.colsurfa.2017.02.006.

(65) Al-Shalabi, E. W.; Sepehrnoori, K. A Comprehensive Review of Low

Salinity/Engineered Water Injections and Their Applications in Sandstone and Carbonate Rocks. *J. Pet. Sci. Eng.* **2016**, *139*, 137–161. https://doi.org/10.1016/j.petrol.2015.11.027.

(66) Katende, A.; Sagala, F. A Critical Review of Low Salinity Water Flooding: Mechanism, Laboratory and Field Application. *Journal of Molecular Liquids*. 2019. https://doi.org/10.1016/j.molliq.2019.01.037.

(67) Li, H.; Vovusha, H.; Sharma, S.; Singh, N.; Schwingenschlögl, U. Mechanism of Wettability Alteration of the Calcite {10$\bar{1}$4} Surface. *Phys. Chem. Chem. Phys.* **2020**, *22* (27), 15365–15372. https://doi.org/10.1039/D0CP01715A.

(68) Fathi, S. J.; Austad, T.; Strand, S. Water-Based Enhanced Oil Recovery (EOR) by "Smart Water": Optimal Ionic Composition for EOR in Carbonates. *Energy and Fuels* **2011**, *25* (11), 5173–5179. https://doi.org/10.1021/ef201019k.

(69) Austad, T.; Shariatpanahi, S. F.; Strand, S.; Black, C. J. J.; Webb, K. J. Conditions for a Low-Salinity Enhanced Oil Recovery (EOR) Effect in Carbonate Oil Reservoirs. *Energy & Fuels* **2012**, *26* (1), 569–575. https://doi.org/10.1021/ef201435g.

(70) Ding, H.; Mettu, S.; Rahman, S. Probing the Effects of Ca2+, Mg2+, and SO42-on Calcite-Oil Interactions by "Soft Tip" Atomic Force Microscopy (AFM). *Ind. Eng. Chem. Res.* **2020**. https://doi.org/10.1021/acs.iecr.0c01665.

(71) Zhang, P.; Tweheyo, M. T.; Austad, T. Wettability Alteration and Improved Oil Recovery in Chalk: The Effect of Calcium in the Presence of Sulfate. *Energy and Fuels* **2006**, *20* (5), 2056–2062. https://doi.org/10.1021/ef0600816.

(72) Strand, S.; Høgnesen, E. J.; Austad, T. Wettability Alteration of Carbonates - Effects of Potential Determining Ions (Ca2+ and SO42-) and Temperature. *Colloids and Surfaces A: Physicochemical and Engineering Aspects*. 2006, pp 1–10.

https://doi.org/10.1016/j.colsurfa.2005.10.061.

(73) Rezaei Gomari, K. A.; Denoyel, R.; Hamouda, A. A. Wettability of Calcite and Mica Modified by Different Long-Chain Fatty Acids (C18acids). *J. Colloid Interface Sci.* **2006**, *297* (2), 470–479. https://doi.org/10.1016/j.jcis.2005.11.036.

(74) Xie, Y.; Khishvand, M.; Piri, M. Wettability of Calcite Surfaces: Impacts of Brine Ionic Composition and Oil Phase Polarity at Elevated Temperature and Pressure Conditions. *Langmuir* **2020**. https://doi.org/10.1021/acs.langmuir.0c00367.